

A STUDY OF CARBON FEATURES IN TYPE IA SUPERNOVA SPECTRA

JEROD T. PARRENT¹, R. C. THOMAS², ROBERT A. FESEN¹, G. H. MARION^{3,4}, PETER CHALLIS³, PETER M. GARNAVICH⁵,
DAN MILISAVLJEVIC¹, JÖZSEF VINKÒ⁶, J. CRAIG WHEELER⁴

Submitted to the Astrophysical Journal 2010 December 1; accepted 2011 February 28

ABSTRACT

One of the major differences between various explosion scenarios of Type Ia supernovae (SNe Ia) is the remaining amount of unburned (C+O) material and its velocity distribution within the expanding ejecta. While oxygen absorption features are not uncommon in the spectra of SNe Ia before maximum light, the presence of strong carbon absorption has been reported only in a minority of objects, typically during the pre-maximum phase. The reported low frequency of carbon detections may be due to low signal-to-noise data, low abundance of unburned material, line blending between C II λ 6580 and Si II λ 6355, ejecta temperature differences, asymmetrical distribution effects, or a combination of these. However, a survey of published pre-maximum spectra reveals that more SNe Ia than previously thought may exhibit C II λ 6580 absorption features and relics of line blending near \sim 6300 Å. Here we present new SN Ia observations where spectroscopic signatures of C II λ 6580 are detected, and investigate the presence of C II λ 6580 in the optical spectra of 19 SNe Ia using the parameterized spectrum synthesis code, *SYNOW*. Most of the objects in our sample that exhibit C II λ 6580 absorption features are of the low-velocity gradient subtype. Our study indicates that the morphology of carbon-rich regions is consistent with either a spherical distribution or a hemispheric asymmetry, supporting the recent idea that SN Ia diversity may be a result of off-center ignition coupled with observer line-of-sight effects.

Subject headings: supernovae: general — supernovae: individual (SN 2010Y, 2010ai, PTF10icb)

1. INTRODUCTION

The typical pre-maximum SN Ia spectrum consists of overlapping P-Cygni profiles of intermediate-mass elements (IMEs) and Fe-peak elements (IPEs) that indicate expansion velocities on the order of 10^4 km s⁻¹ (Filippenko 1997). Photometric properties of the rise, peak, and decline of a SN Ia light curve can be explained by assuming that a substantial amount of ⁵⁶Ni, synthesized in the explosion, powers the SN luminosity (Colgate & McKee 1969; Arnett 1982). Consequently, results of spectroscopic and photometric studies have supported the idea that SNe Ia are the outcome of a thermonuclear explosion of a C+O white dwarf in a binary system (Hoyle & Fowler 1960; Nomoto et al. 1984; Elias et al. 1985; Iben 1988; Nomoto et al. 2003; Chen & Li 2009; Howell 2010).

The explosion mechanisms that have been proposed differ by how the thermonuclear flame is propagated through the star's interior; i.e., a sub-sonic deflagration via thermal conductivity or a super-sonic detonation due to strong shock burning. Pure detonation models appear unlikely since they conflict with observations by producing too much ⁵⁶Ni, not enough IMEs, and leaving very little unburned material behind (Arnett 1969;

Branch & Khokhlov 1995). On the other hand, while pure deflagration models may account for fainter SN Ia events, they are energetically weak, leaving too much material unburned to represent the majority of SNe Ia (Travaglio et al. 2004; Gamezo et al. 2005; Kozma et al. 2005). Thus, a deflagration that transitions into a detonation may be necessary in order to attain the nucleosynthetic yields that are consistent with the observations (Khokhlov 1991; Höflich et al. 1995; Kasen et al. 2009; Maeda et al. 2010a).

Additional facets of modeling (e.g., multidimensional considerations) will affect the abundance tomography as well (Woosley et al. 2009). This can make it difficult to distinguish the dominant sources of SN Ia diversity. For certain, however, one similarity between all explosion models is the existence of burned (ash) and unburned material (fuel). By using spectroscopic signatures of C and O at pre-maximum epochs, one can infer the amount and velocity structure of the outer, unburned material.

Some of the unburned material may be subject to a degree of downward mixing toward the inner ejecta when burning becomes turbulent and enters the distributed flame regime (Pope 1987; Niemeyer 1998; Aspden et al. 2010). As a result, it is not certain whether regions of unburned material are strictly located in the outer layer or mixed within the rest of the ejecta, nor is the mass range of unburned material from these thermonuclear explosions known (Baron et al. 2003). Therefore, the rate of detection of unburned material and its phenomenological details is of great importance for constraining how much material remains unburned in the explosion models.

The most prominent oxygen line in the optical spectra of SNe Ia is O I λ 7774. Unfortunately, since oxygen is a product of carbon burning, oxygen absorption lines are

¹ 6127 Wilder Lab, Department of Physics & Astronomy, Dartmouth College, Hanover, NH 03755, USA.

² Physics Division, Lawrence Berkeley National Laboratory, 1 Cyclotron Road, Berkeley, CA 94720, USA.

³ Harvard-Smithsonian Center for Astrophysics, 60 Garden St., Cambridge, MA 02138, USA.

⁴ Astronomy Department, University of Texas at Austin, Austin, TX 78712, USA.

⁵ Physics Department, University of Notre Dame, Notre Dame, IN 46556, USA.

⁶ Department of Optics & Quantum Electronics, University of Szeged, Dòm tèt 9, Szeged H-6720, Hungary.

likely to be a biased reference for measuring the location of unburned material. Thus one must look to carbon absorption features as a tracer for unburned material. While it is not uncommon for oxygen to be present in SN Ia spectra (Branch et al. 2006), signatures of carbon have only been sporadically reported in SN Ia spectra, most often during the pre-maximum phase.

For the typical ejecta temperatures seen in SNe Ia ($\sim 10,000$ K), the dominant ionization state of carbon is C II (Tanaka et al. 2008). At this temperature, the strongest optical line of C II is that of $\lambda 6580$ (Hatano et al. 1999b). When seen, this line produces a blue-shifted absorption near 6300 \AA that sometimes blends with the neighboring emission component of the Si II $\lambda 6355$ P-Cygni profile, thus making C II identifications problematic. There are well observed SNe Ia where C II $\lambda 6580$ is clearly present (Patat et al. 1996; Mazzali 2001; Garavini et al. 2005; Hicken et al. 2007; Thomas et al. 2007; Yamanaka et al. 2009b; Scalzo et al. 2010), however in general, C II absorption is often weak and/or blended and therefore not a conspicuous SN Ia feature (Salvo et al. 2001; Branch et al. 2003; Stanishev et al. 2007).

A number of factors intrinsic to the explosion itself may contribute to the strength of C II $\lambda 6580$ and whether or not carbon features show up in SN Ia spectra. These include the asymmetrical distribution of carbon, the extent of carbon burning, the temperature of the carbon-rich region, and the possible formation of an envelope of unburned material through a merger of two white dwarfs (Thomas et al. 2007; Tanaka et al. 2008; Scalzo et al. 2010). Low signal-to-noise spectra and effects of line formation may also obscure weak C II $\lambda 6580$ absorption features, thereby complicating the rate of detection further.

In an attempt to better understand spectroscopic carbon signatures in the pre-maximum optical spectra of SNe Ia, we present a comparative study of 16 SNe Ia where a C II $\lambda 6580$ absorption signature is evident, plus three additional cases where it may be present. Then using the spectrum synthesis code, *SYNOW*, we fit this sample of SN Ia spectra thereby mapping the velocity distribution of carbon-rich regions that give rise to C II $\lambda 6580$ absorption features. To ensure a consistent analysis, we generated synthetic spectra for each of the time-series spectra in our sample.

The new and archival data used in this study are presented in §2. We review SN Ia subtype classifications in §3, and in §4 we discuss the spectrum fitting methods implemented with the *SYNOW* model, followed by our results in §5. We discuss our results in §6 in the context of recent findings on the diversity of SNe Ia and conclude in §7 with our results regarding the nature of C II absorption features.

2. DATA

Low signal-to-noise (S/N) SN Ia spectra make investigations of any suspected C II absorption features difficult. Therefore, with the possibility of carbon features being both weak and blended with Si II $\lambda 6355$, well observed multi-epoch confirmations of any suspected C II $\lambda 6580$ signatures were preferred for analysis.

In constructing our data sample, we have included only SNe Ia where at least two consecutive spectra showed the

presence of a $\sim 6300 \text{ \AA}$ absorption signature, indicating a likely C II $\lambda 6580$ absorption feature. In addition, if the C II feature was not seen before maximum light, then we did not include those SNe in our sample since this region of the spectrum becomes contaminated by neighboring Fe II lines within a week after maximum light (Branch et al. 2008). The two exceptions are the single epoch spectra of PTF10icb and the 2002cx-like, SN 2008ha, where the C II $\lambda 6580$ signature is evident.

2.1. New Observations

Pre-maximum optical spectra of SN 2010Y, 2010ai, and PTF10icb show absorptions likely due to C II $\lambda 6580$ and thus we included these in our sample. These data were reduced using standard IRAF procedures, were corrected for host galaxy redshift and are presented in Figure 1 and Table 1. We used the spectrum-comparison tool, SNID (Blondin & Tonry 2007), to estimate the age of each spectrum relative to maximum light.

Three spectra for SN 2010Y covering days -7 , -6 , and -3 with respect to maximum light were obtained using a Boller & Chivens CCD spectrograph (CCDS) on the 2.4 m Hiltner telescope at the MDM Observatory on Kitt Peak, Arizona. These spectra show the emergence of a relatively weak yet persistent 6330 \AA absorption feature. Two additional spectra were taken on day -2 and $+1$ and were acquired with the 9.2 m Hobby-Eberly Telescope (HET) (Ramsey et al. 1998) at the McDonald Observatory using the Marcario Low-Resolution Spectrograph (LRS, Hill et al. 1998). By day -2 , the 6330 \AA feature peaked in intensity and began to fade by day $+1$.

Low resolution optical spectra of SN 2010ai were also obtained with HET. Spectra were taken well before maximum light on days -10 and -8 . These spectra show signs of a flux depression in the emission component of the Si II $\lambda 6355$ P-Cygni profile, suggesting the presence of C II $\lambda 6580$ absorption.

Additional data comes from the discovery of PTF10icb by The Palomar Transient Factory (Nugent et al. 2010). A low-resolution follow-up spectrum was obtained with the LRS on HET on June 3. The spectrum-comparison tool, SNID, identifies the spectrum of PTF10icb as that of a normal SN Ia near day -10 . Similar to SN 2010Y and 2010ai, the spectrum of PTF10icb also exhibited a 6330 \AA absorption feature.

2.2. Archival Data

In Table 2, we list these three recent objects alongside 65 SNe Ia found in the literature with pre-maximum or near maximum light spectra. These 68 SNe have been organized by the subtype scheme of Benetti et al. (2005) and are labeled by the classification subtypes of Branch et al. (2006) (see §3). Since the progenitor channel and the origin of C II $\lambda 6580$ absorption features may differ for Super-Chandra SNe Ia, we separate SN 2003fg, 2006gz, 2007if and 2009dc as possible Super-Chandra candidates. We have also grouped SN 2000cx, 2002bj, 2002cx, 2007qd and 2008ha as miscellaneous objects since their classifications as SN Ia-like events are still under debate (Valenti et al. 2009; McClelland et al. 2010; Poznanski et al. 2010).

Optical spectra for all but three SNe Ia in our sample were obtained from the Supernova Spectrum Archive

(SuSpect¹) and sources therein. All spectra have been corrected for host galaxy redshift and normalized according to the formula given by Jeffery et al. (2007) in order to remove the underlying continuum since in this study we are only concerned with the position of the C II $\lambda 6580$ absorption minimum and not absolute flux. The inclusion of SN 2008ha is for comparison purposes only and not meant to contribute to the discussion of carbon-rich regions of normal SNe Ia.

In Figure 2, we present a single pre-maximum spectrum of the 19 SNe Ia in our sample that show evidence of a C II $\lambda 6580$ absorption signature. Under the assumption of local thermodynamic equilibrium at 10,000 K, the strongest four optical lines of C II are $\lambda\lambda 4267, 4745, 6580,$ and 7234 , with the 6580 \AA line being the strongest. Rest frame positions of these lines are represented as vertical lines in Figure 2 and the four grey bands at the top indicate Doppler velocities of $1000\text{--}20,000 \text{ km s}^{-1}$. This corresponds to a region spanning 440 \AA wide and blueward of 6580 \AA , well within the extent of typical Si II $\lambda 6355$ P-Cygni profiles.

In Table 2 we also note the epoch of the earliest spectrum taken and how likely a C II $\lambda 6580$ detection is for each SN Ia (see §5.2). If both C II $\lambda 6580$ and $\lambda 7234$ absorption features are present or if the C II $\lambda 6580$ is an obvious notch, then we denote the detection as “Definite”. If a weaker notch is seen, and both absorption wings remain, then the detection is labeled as “Probable”. If a $\sim 6300 \text{ \AA}$ feature comes in the form of a “slump” on the emission component of Si II $\lambda 6355$, then we note the C II $\lambda 6580$ detection as “Possible”. Some of the published data have S/N ratios that prevent making a clear case for C II $\lambda 6580$ detection and we note these as “Uncertain”. If none of these criteria are met, then there is “No” detection.

3. SNE IA: SUBTYPE CLASSES

The observed diversity of SNe Ia has been subdivided based on photometric and spectroscopic properties by Benetti et al. (2005) and Branch et al. (2006). Below we briefly describe these classification schemes which will be referred to in our analysis.

Benetti et al. (2005) grouped 26 SNe Ia according to two photometric and three spectroscopic observables, namely (1) $\Delta m_{15}(B)$ – the decline in magnitude of the B-band 15 days after B-band maximum (Phillips 1993), (2) M_B – the peak B-band magnitude, (3) \dot{v}_{SiII} – the Si II expansion velocity rate of decrease, (4) $v_{10}(\text{Si II})$ – the expansion velocity of Si II $\lambda 6355$ 10 days after maximum light, and (5) $\mathcal{R}(Si)_{max}$ – the ratio of $\lambda\lambda 5972, 6355$ absorption depth measured at maximum light (Nugent et al. 1995; Bongard et al. 2008).

With a sample of 26 SNe Ia, they found that SNe Ia could be organized into three discrete subtypes that were functions of velocity gradient and luminosity, namely (1) high-velocity gradient (HVG), (2) low-velocity gradient (LVG), and (3) FAINT. The subtypes HVG and LVG were mainly distinguished by having \dot{v} values above or below $\sim 70 \text{ km s}^{-1} \text{ day}^{-1}$, respectively, while the SNe in their sample with $M_{B,max} \gtrsim -18.20$ were labeled as FAINT.

Branch et al. (2006) took a purely spectroscopically based approach, classifying 24 SNe Ia (later 65 SNe; see Branch et al. 2009) by the equivalent width of features near 5750 \AA and 6100 \AA which are usually attributed to Si II $\lambda\lambda 5972, 6355$, respectively. When SNe Ia are arranged in this manner, the objects can be subdivided roughly into four spectroscopic subtypes: (1) Core-Normal (CN) SNe Ia consist of objects such as SN 1994D, where from pre-maximum to 1-week post-maximum spectra are dominated by lines of Ca II, Fe II, Fe III, Mg II, O I, S II, Si II, and Si III, (2) Broad-Line (BL) SNe Ia are similar to CNs but instead display noticeably broader lines with higher average Doppler velocities, (3) Cool (CL) 1991bg-like spectra which exhibit low ionization energy ions such as Ti II, along with an increased ratio between the 5750 and 6100 \AA features, and (4) Shallow Silicon (SS) 1991T-like display mostly high ionization energy ions, such as Fe III, in their pre-maximum spectra and are accompanied by weak S II absorption features.

We note that comparing the sample of SNe Ia used in both studies shows that FAINT and HVG objects are equivalent to CL and BL respectively, and the LVG objects are equivalent to CN and SS subtypes (Branch et al. 2006). Since we are using subtype classes that are mostly based on spectroscopic properties of SNe Ia, our study cannot address issues regarding broadband photometric observations. A systematic study of both the spectroscopic and light-curve properties is difficult because these data can come from multiple sources and not every target we study here have both good spectroscopy and photometry. This type of study is better suited for the Nearby Supernova Factory (Aldering et al. 2002) and the Palomar Transient Factory (Rau et al. 2009), where the data sets are large and have good time-series coverage.

4. SPECTRUM ANALYSIS MODEL: SYNOW

One way to infer the velocity range of unburned material is to measure the absorption minimum of the C II $\lambda 6580$ line. The observed minimum of this feature is often located near the strong emission component of Si II $\lambda 6355$, and is therefore subject to line blending and any limb-brightening that the Si II line contributes to the integrated spectrum (Höflich 1990). Consequently, the observed minimum may underestimate the actual expansion velocity of the carbon-rich region. Therefore, in order to accurately estimate the true minimum of a blended line profile, one must take into account the effects of line formation by reconstructing the spectrum via numerical calculation.

While there have been several new and more detailed spectrum synthesis codes presented in the literature since the inception of SYNOW nearly thirty years ago, the SYNOW spectrum synthesis model remains a useful tool for the quick analysis of resonant scattering line profiles (Baron et al. 1994; Mazzali 2000; Branch et al. 2007; Kasen et al. 2008; Baron et al. 2009). Therefore, we chose the less computationally intensive approach of SYNOW to produce results that were internally consistent when we compared the SNe Ia in our sample.

From a single-epoch optical spectrum, one can reproduce many of the conspicuous features seen in SNe Ia of all subtypes using SYNOW. However, to have greater confidence in the identification of a spectroscopic feature,

¹ <http://nhn.ou.edu/~suspect>

it is best to have a time series of closely spaced spectra in order to follow the evolution of both the observations and the fit. Because we wish to probe the nature of C II $\lambda 6580$ features in SNe Ia, we required fitting all spectra for the duration of time in which the 6300 Å features could be seen.

In *SYNOW*, one computes a spectrum by specifying the location and optical depth for a given set of ions. This allows one to infer spectral line identifications by directly fitting to a series of observed spectra. While *SYNOW* does not calculate relative abundances of various elements, it is instructive at reconstructing the complex spectroscopic profiles brought about by multiple line scattering that is inherent to moving media.

The version of the *SYNOW* model that we used can be described as follows: (1) a spherically symmetric and homologously expanding ejecta is modeled using a $v \propto r$ law, (2) light is emitted from a sharp photosphere, (3) optical depth, τ , is a function of velocity as either

$(v/v_{phot})^{-n}$, $exp^{-\frac{v-v_{phot}}{v_e}}$, or $exp^{-\frac{(v-v_{phot})^2}{2\sigma^2}}$ where each of these functions are characterized by indices n , v_e , and σ respectively, (4) line formation is purely due to resonant scattering and is treated using the Sobolev Approximation (Sobolev 1957; Jeffery & Branch 1990), and (5) for a given ion a reference line profile is calculated for a given τ and the remaining lines follow from Boltzmann statistics. Input parameters for a *SYNOW* spectral fit include: (i) a photospheric velocity (v_{phot}), (ii) reference line τ and minimum/maximum velocities for each ion, and (iii) excitation temperature, T_{exc} , to determine LTE level populations with respect to a reference line.

As was done in the SN Ia comparative study of Branch et al. (2005), for our investigation we too left the excitation temperature at 10,000 K for each ion. We also chose to use the exponential form of the optical depth profile with $v_e = 1000 \text{ km s}^{-1}$. This aided in limiting the number of free parameters for a spectral fit.

Because *SYNOW* assumes spherical symmetry, we are limited when investigating the possible asymmetrical distributions of unburned material. If the distribution is that of a spherical layer, as is the case for the W7 model (Nomoto et al. 1984; Thielemann et al. 1986), then it is straightforward to make *SYNOW* model fits to compare with observations. In this case, the unburned material resides above the burned material in a spherical shell where the thickness depends on the extent of the burning. For W7, this boundary is roughly at $14,000 \text{ km s}^{-1}$ with a stratified composition of IMEs and IPEs below.

Recent multidimensional models of delayed detonations suggest that the unburned material may be left behind in clumps throughout the ejecta (Gamezo et al. 2004). For the situation where the unburned material is heavily concentrated to a single clump structure, we can only utilize *SYNOW* in certain cases (see §5.4).

Observations have shown that there often exists higher velocity regions of line formation; namely Ca II and Si II (Hatano et al. 1999a; Kasen et al. 2003; Tanaka et al. 2010). Such regions are said to be *detached* from the photosphere. We note a noticeable facet that arises when fitting Si II $\lambda 6355$ profiles during the earliest epochs is that the absorption width, the slow rise of the blue wing, and the sharp rise of the red wing require two separate velocity components of Si II to achieve a good match to

observations. At best, a single-component of Si II with an increased value of the optical depth profile indices can only properly fit the red wing of the 6355 Å absorption feature.

G. H. Marion et al. (2011, in preparation) discuss recent observations of the Type Ia event, SN 2009ig, where there is clear evidence for both a photospheric region and a high velocity region of Si II. In their *SYNOW* analysis, they used the two-component approach in following the evolution of the Si II $\lambda 6355$ feature, which produced a better fit overall. Similarly, we too have adopted a procedure of using two components of Si II that are separated by $\sim 4000\text{--}6000 \text{ km s}^{-1}$ when necessary.

One consequence that detached ions have on the line profile is that the emission component of the line is flat-topped. Some of our spectroscopic fits in §5.3 detach Si II to better fit the absorption component, while forfeiting a comparable fit to the full emission component; e.g. our fit for SN 1999ac. The impact that detaching has towards blending with C II $\lambda 6580$ is minimal and only one of offsetting the prescribed value of τ for C II in the fit.

5. RESULTS

In terms of the spectroscopic diversity of SNe Ia, many of the differences are seen immediately after the explosion as the photosphere maps out the distribution of the outermost ejected material, with an increase toward spectroscopic conformity at later epochs (Branch et al. 2008). Unfortunately, as shown in Figure 3, SN Ia spectroscopic observations during the two weeks prior to maximum light are underrepresented compared to those taken near maximum light or at later times. In addition, absorption features attributed to C II $\lambda 6580$ are generally weak. As a result, they can be easily missed and thus go unreported or are not securely verifiable due to low S/N and/or line blending.

5.1. Frequency of C II Absorption Features

Our search of the literature revealed that $\sim 30\%$ of SNe Ia with moderate to high S/N, pre-maximum spectra taken since 1983 January 1 show a feature near 6300 Å that may be associated with C II $\lambda 6580$ absorption (see Table 2; Definite + Probable). Because of the sparsity of optical spectra before peak brightness, this percentage may not represent the actual fraction of SNe Ia that exhibit C II $\lambda 6580$ signatures during the pre-maximum phase. Furthermore, the amount of published SN Ia data does not equal the amount of data taken, thereby placing considerable uncertainty on such an estimate.

For comparison, in Figure 3, we also tally and plot the total number of SNe Ia where C II $\lambda 6580$ was first detected with respect to maximum light. When the total number of published C II observations over the past couple decades is compared to the total number of SNe Ia discovered during the pre-maximum phase in a span of three years, the occurrence of absorption due to C II $\lambda 6580$ appears infrequent.

However, many SNe Ia might show C II (or C I, or C III; see §6.1) during the first weeks of the explosion, but may not exhibit strong, identifiable carbon absorption features by the time they are discovered and spectra taken. If spectra are not obtained prior to maximum light, this can lead to an under-reporting of C II SNe Ia

cases. For example, in some objects, the C II features appear to fade by day -5 or even earlier. This raises the question: Might all SNe Ia show appreciable C II absorption at some level if observed at a sufficiently early enough epoch?

Given the weak impact that C II features are observed to have on the integrated optical spectrum, identifying every instance for when C II is present rests heavily on one’s ability to distinguish the signature from noise and the effects of line blending. In Figure 4, we compare the spectrum of SN 1998aq at day -9 to three cases where we have artificially added Gaussian noise to the original spectrum. With only 10% and 20% noise added, the C II $\lambda 6580$ feature remains distinguishable. However, at 25% the feature begins to lose its identity above the noise. An example of this is the spectrum of SN 2005bl at day -6 , shown in Figure 4. Taubenberger et al. (2008) proposed a C II $\lambda 6580$ identification for the 6400 Å depression seen in the spectrum. However, we excluded this SN from our sample since we were not able to generate an accurate fit for the feature.

5.2. SNe Ia C II Features: Conspicuous to Weak

Like most features in the spectra of SNe Ia, the degree of adjacent line blending that C II $\lambda 6580$ absorption signatures undergo can obscure the full extent of a line profile. More often than not, the minimum of the C II $\lambda 6580$ line is blended with the P-Cygni emission component of the Si II $\lambda 6355$ line. The day -5 spectrum of SN 1999by is a good example of when this takes place (see Figure 2).

When the C II $\lambda 6580$ absorption feature is weak there is also often no obvious C II $\lambda 7234$ signature. However, when the C II $\lambda 6580$ feature is strong, a corresponding C II $\lambda 7234$ feature does begin to appear as the excited level of the 7234 Å line becomes more populated. There are several cases, such as SN 2006gz and 2007if, where C II $\lambda 6580$ is certainly present but either the wavelength coverage is incomplete or the spectrum is too noisy to say whether or not C II $\lambda 7234$ is present as well.

In Figure 5, we plot two spectral regions of four SNe Ia in Figure 2 that highlight cases when both of these C II lines are present. For each SN, the red and blue lines denote $\lambda\lambda 6580, 7234$ Doppler velocity-scaled spectra, respectively. The absorption minima overlap nicely (see dashed vertical lines) and the symmetry about the minima is indicative of a match between the spectral signatures of the same ion. We interpret this to mean that the 7234 Å line is indeed present when the 6580 Å line is strong. Currently, these two C II lines are the best means by which to securely identify whether carbon is present in the early-epoch SN Ia spectra.

The C II lines that appear further in the blue have also been suggested to be present as well (Thomas et al. 2007). However, this region is crowded by lines of IPEs making it more difficult to securely identify C II $\lambda\lambda 4267, 4745$ and use for determining accurate Doppler velocities. This appears to even be the case for SN 2006gz, 2007if, and 2009dc where the C II $\lambda 6580$ absorption is strong (Hicken et al. 2007; Scalzo et al. 2010; Taubenberger et al. 2011).

5.3. SYNOW Model Fitting

For each of the 19 SNe Ia in our C II sample, we produced a time series of synthetic optical spectra that covered the observed extent of the C II $\lambda 6580$ feature’s presence as well as the observed wavelength coverage of the data ($\sim 3500\text{--}9000$ Å). Our initial fits included the canonical set of IMEs and IPEs that are prevalent in pre-maximum SN Ia spectra, whereby afterward we included C II and adjusted the optical depth and detachment velocity until a match to observation was made. The goodness-of-fit to the observed Si II $\lambda 6355$ – C II $\lambda 6580$ blended profiles did not change with the full set of IMEs and IPEs removed. Thus, for each SN in Table 3, we only list the relevant parameters for C II and Si II.

As was discussed above in §4, some of the observed Si II $\lambda 6355$ profiles required two separate components of Si II in order to fit the full width of the absorption. We indicate which SNe Ia in our sample required this fitting procedure by appending the inferred Doppler velocities and optical depths with “>” in Table 3.

In Figure 6, we compare fits to a single observed spectrum for each of the SNe Ia in our sample. The black lines represent the observed spectra, the red lines are SYNOW fits where C II has been included, and the blue lines are the same fits without C II. The synthetic spectra match fairly well to a variety of Si II $\lambda 6355$ – C II $\lambda 6580$ blended profiles, and the interpretation that the 6300 Å feature is due to C II $\lambda 6580$ is in agreement with that of previous authors (see references in Table 2).

In this study, we also offer new and revised expansion velocity estimates of C II for a couple SNe Ia, particularly SN 1990N and 1999by. It was suggested by Fisher et al. (1997) that the overly broadened 6040 Å absorption in the day -14 spectrum of SN 1990N was due to a two-component blend composed of Si II at $\sim 20,000$ km s $^{-1}$ and C II at $\sim 26,000$ km s $^{-1}$. Similarly, Mazzali (2001) suggested that this feature is predominantly due to Si II $\lambda 6355$ but also requires an outer zone of high velocity carbon between 19,000 and 30,000 km s $^{-1}$. If this interpretation is correct, then other SNe Ia like SN 1990N would also require a similar zone of carbon to reproduce their early-epoch spectra. However, our fit for SN 1990N uses two components of Si II to fill the 6040 Å feature while C II is only at 16,000 km s $^{-1}$ to account for the 6300 Å feature.

In the case of the sub-luminous SN 1999by, C II $\lambda 6580$ was not reported by Garnavich et al. (2004). However, our fit in Figure 6 is fairly convincing when C II is included as a detached layer 2000 km s $^{-1}$ above the photosphere for the day -5 spectrum. In fact, almost 80% of the SNe in our sample suggest at least a mildly detached layer of C II during some point along the evolution of the absorption feature. For example, we modeled the C II in SN 1994D initially at 14,000 km s $^{-1}$ coincident with v_{phot} at day -11 , after which it remains at this velocity as the photosphere recedes to 12,000 km s $^{-1}$ by day -5 .

6. DISCUSSION

The strength and velocity range of carbon in pre-maximum SNe Ia spectra can provide a valuable tool to investigate various explosion models. The W7 deflagration model, for instance, contains a $\sim 0.07M_{\odot}$ layer of unburned material above 14,000 km s $^{-1}$. Using the spectrum synthesis and model atmosphere code, PHOENIX,

Lentz et al. (2001) compared calculated non-LTE spectra to spectroscopic observations of the normal Ia event, SN 1994D. Despite the outer layer of unburned material in W7, none of their synthetic spectra were able to account for the observed C II $\lambda 6580$ absorption feature near 6290 \AA . Our SYNOW fits for this object allow for C II below $14,000 \text{ km s}^{-1}$. To that end, Tanaka et al. (2011) were able to reproduce a C II $\lambda 6580$ absorption feature seen in the day -11 spectrum of SN 2003du by placing the carbon-rich region at lower velocities in their version of W7. They obtained an upper limit on the abundance of carbon to be $0.016 M_{\odot}$ at $v > 10,500 \text{ km s}^{-1}$ in this object.

At late-times and based on the three-dimensional deflagration models of Röpke (2005), Kozma et al. (2005) compared synthetic spectra to the late-time spectra of three SNe Ia and set an upper mass limit of unburned material below $10,000 \text{ km s}^{-1}$ to be $\sim 0.07 M_{\odot}$. Other estimates for the mass of unburned material have been made using delayed-detonations (Höflich et al. 2002) and other modeling; e.g. lower limit of $0.014 M_{\odot}$ of unburned material between $10,000$ and $14,000 \text{ km s}^{-1}$ for SN 2006D (Thomas et al. 2007). However, since each estimate is obtained by different means, a comparison of such results does not advance the discussion on the nature of C II $\lambda 6580$ absorption features.

In order to utilize C II $\lambda 6580$ absorption features for estimating the mass of unburned material, the effects of temperature and geometry of the carbon-rich regions as well as the influence of radiative transfer effects must be explored. Our SYNOW modeling begins this process by mapping the observed velocity distribution for a sample of 19 SNe Ia. Below, we discuss our interpretation of the observed frequency of C II absorption features and how they relate to the properties of carbon-rich regions and SN Ia diversity.

6.1. Temperature Effects on Carbon Features

The temperature of the carbon-rich region will influence whether or not C II is the dominant ionization species and will therefore dictate the strength of C II $\lambda 6580$ absorption features. Using non-LTE calculated spectra, Nugent et al. (1995) pointed out that the spectroscopic sequence observed among various SNe Ia could be explained by a continuous change in the effective temperature of the ejecta (7400 – $11,000 \text{ K}$), from cool 1991bg-likes to the hotter 1991T-likes (see their Fig. 1). While the ejecta of SNe Ia are an environment with non-LTE processes, under the assumption of a C+O-rich composition the Saha-Boltzmann equation indicates that carbon will mostly be in the form of C II between 6000 and $12,000 \text{ K}$.

Of the 68 SNe Ia listed in Table 2, 10 out of the 14 CNs and five out of the 13 CLs exhibit C II $\lambda 6580$ absorption features. From a nearly equal sampling of SN Ia subtypes, the fact that two CNs for every one CL SN Ia exhibit C II absorption lines suggests that the presence of C II absorption features depend on the effective temperature to some degree. This point is also consistent with the fact that only two of 13 SSs show signs of C II $\lambda 6580$ absorption features in their spectra.

We note that C I absorption features are not often detected in SN Ia spectra. Marion et al. (2006) presented NIR spectra of three normal SNe Ia and discussed the

lack of C I absorption signatures due to the absence of the strongest C I NIR lines, namely C I $\lambda \lambda 9093, 10691$. A more extensive study of 41 SN Ia NIR spectra spanning two weeks before and after maximum light was discussed by Marion et al. (2009) and they too reported a lack of C I signatures. Because spectral signatures of carbon burning products were observed to occupy the same region of ejecta (Mg II and O I), Marion et al. (2006) concluded that nuclear burning had been complete out to at least $18,000 \text{ km s}^{-1}$ in their objects.

It is perhaps not surprising that many NIR spectra of SNe Ia do not show lines from C I, given that (1) the abundance of carbon may be only ~ 1 - 10% of the total ejected mass, and (2) if there is carbon present in the outer layers then it is mostly once ionized. Interestingly, however, Höflich et al. (2002) reported a conspicuous C I $\lambda 10691$ absorption feature in the day -4 NIR spectrum of SN 1999by. They were able to reproduce many features of the observed optical and NIR spectra using a series of sub-luminous delayed-detonation models with a range of transition densities, ρ_{tr} , between 8 – $27 \times 10^6 \text{ g cm}^{-3}$.

The appearance of the C I $\lambda 10691$ line was seen concurrently with the optical C II $\lambda 6580$ absorption feature we reported above in §5.3. Both the C I and C II spectral signatures indicated that the carbon-rich region was above the $12,000 \text{ km s}^{-1}$ photosphere; i.e. the minimum of the C I $\lambda 10691$ absorption corresponds to $\sim 13,000 \text{ km s}^{-1}$ while our SYNOW fits for this object place C II at $14,500 \text{ km s}^{-1}$. At least for this cool sub-luminous SNe Ia, the influence of temperature on the ionization state of the carbon-rich region is apparent from the simultaneous appearance of C I and C II absorption features.

Additional evidence that ejecta temperature plays a role in the detection of carbon in SN Ia spectra would be if C III were clearly detected in a hotter SN Ia subtype, such as SN 1991T or SN 1997br. The similarity between the ionization potentials of C II (24.4 eV) and S II (23.3 eV) suggests that the presence of C III absorption features may be concurrent with spectroscopic signatures of S III. Fortunately, we can examine optical spectra to check for the simultaneous presence of C III $\lambda 4649$ and S III $\lambda 4254$ absorption features.

In Figure 7, we plot and compare SYNOW fits for SN 1991T and 1997br where we have included C III and S III. The identification of the 4500 \AA feature of SN 1991T has been discussed before by Hatano et al. (2002), and similarly in other SN Ia (Garavini et al. 2004; Chornock et al. 2006). While it was argued by Hatano et al. (2002) that including C III in the fit produced a mis-match with the observed spectrum (too blue overall), our synthetic spectra (red lines) are in fair agreement with observations near 4500 \AA for both SN 1991T and 1997br.

In addition, a better fit to the 4250 \AA absorption feature is obtained with the inclusion of S III. The 4250 \AA feature is predominately due to the Fe III $\lambda 4404$ multiplet. However, by adding S III to the fit we were able to fill in the blue wing of this absorption feature for both objects. Therefore, our identification for the 4500 \AA absorption feature as being that of C III $\lambda 4649$ is more likely, though the evidence is circumstantial. If the C III $\lambda 4649$ identification is correct, then this may indicate that a lack of C II (or C I) spectroscopic features do not

necessarily imply the complete burning of carbon in the hotter subtype events.

6.2. Interpreting C II $\lambda 6580$ Doppler Velocities

In this paper, our attention has been primarily focused on carbon-rich regions in the outermost ejecta. The wide range of observed C II Doppler velocities among different SNe Ia suggests a large variation in the extent of carbon burning, with some objects exhibiting *high* velocity carbon while in others the carbon is present at *low* velocities (see Table 3). How high or low is usually in reference to the position of the carbon cut-off seen in the W7 model ($\sim 14,000 \text{ km s}^{-1}$) instead of the kinetic energy of the supernova itself.

6.2.1. Extent of Burning via C II $\lambda 6580$

Given that the characteristic ejecta velocity is proportional to $(E_{kin}/M_{ej})^{1/2}$ (Arnett 1982), a standardized way of looking at the extent of burning is a more appropriate measure for interpreting the range of observed carbon velocities. The 6355 \AA line of Si II has been used as an indicator of the photospheric velocity at early epochs (Jeffery & Branch 1990; Patat et al. 1996). Choosing Si II $\lambda 6355$ over other lines alleviates any difficulty in obtaining Doppler velocities amid too much line blending and allows for consistent time-coverage. This makes the absorption minimum of Si II $\lambda 6355$ a good point of reference for investigating the extent of burning via C II $\lambda 6580$ absorption features before maximum light.

In Figure 8, we have the ratio of Doppler velocities, $v(\text{C II } \lambda 6580)/v(\text{Si II } \lambda 6355)$, derived from our SYNOW fits plotted versus days relative to maximum light. This shows that (1) for an individual SN, the ratio remains at a fairly sustained value over time and (2) the different velocity ratios among the SNe lie roughly within the same region and are similar to within $\pm 10\%$. We have ignored the three outliers because one is in a region of the plot where line blending obscures the supposed C II $\lambda 6580$ detection (SN 2001V; see §6.2.2) and the other two objects suggest that the carbon is clumpy and not along the line-of-sight of the observer (SN 2006bt and SN 2008ha).

The notion of an optically thick photosphere in SNe Ia is generally a good assumption, even though the line forming region may extend 500 km s^{-1} in either direction. Therefore, for a given spectrum, any velocities of an ion that are measured to be fairly below that of the photospheric velocity, v_{phot} , may indicate ejecta asymmetries. That is, any observed discrepancy between v_{phot} and v_{CII} could be explained if the actual velocity of C II is the same as v_{phot} but instead of forming in a shell at the observed velocity, the carbon is in a clump at v_{phot} and offset by an angle, θ , from the line of sight. In particular, we can estimate this projection angle if $v_{CII} < v_{phot}$. For SN 2006bt and SN 2008ha we calculate this projection angle to be $\sim 50^\circ$ and 60° , respectively, where our result for SN 2006bt is in agreement with Foley et al. (2010b).

If the dominant C II behavior is due to asymmetrical distributions of a single localized clump of unburned material, one could expect there to be more scatter below the mean that is presented in Figure 8 since an arbitrary orientation of the clump relative to the observer ought to

lead to more cases where $v(\text{C II } \lambda 6580)/v(\text{Si II } \lambda 6355) < 1$ (like SN 2006bt). Instead, what we find for the SNe in our sample is that the distribution of carbon-rich material is consistent with a layered or hemispheric geometry.

Another surprising aspect of Figure 8 is that the candidate Super-Chandra SNe Ia reside in the same region of the plot as the other objects. Scalzo et al. (2010) suggested that the large C II $\lambda 6580$ feature, concurrent with low velocities, could be explained by invoking a pre-explosion envelope of progenitor material originating from the merger of two white dwarfs. In this scenario, the explosion is inhibited by and loses kinetic energy to the envelope, ionizing the shell of surrounding carbon. Whatever the nature of carbon-rich regions in these three SNe Ia, it is also constrained by the value of $v(\text{C II } \lambda 6580)/v(\text{Si II } \lambda 6355)$.

6.2.2. Consequences of Line Blending

Toward the uppermost region of Figure 8, there is a noticeable lack of highly detached C II objects with time-series coverage that exhibit pre-maximum C II $\lambda 6580$ absorption features. This does not necessarily imply that carbon-rich regions in SNe Ia are absent above a particular velocity. Rather, the “missing” subset of objects may be a result of SNe Ia with lower density carbon-rich regions further out and/or radiative transfer selection effects; e.g. line blending.

Most of the SNe Ia in our sample that exhibit C II $\lambda 6580$ absorption features are of the LVG subtype while only one is an HVG event (SN 2009ig). This is either a real trend of C II $\lambda 6580$ absorption features and therefore a diagnostic of SN Ia diversity, or a result of line blending due to very high velocities of carbon-rich regions. In regards to the latter cause, some SNe Ia might contain a C II $\lambda 6580$ absorption feature in their spectra but its presence is obscured by the Si II $\lambda 6355$ absorption trough, particularly for HVGs.

Assuming that the scatter of $v(\text{C II } \lambda 6580)/v(\text{Si II } \lambda 6355)$ values in Figure 8 is the same for both HVG and LVG subtypes, and assuming that HVGs span a v_{phot} -space from $14,000$ to $16,000 \text{ km s}^{-1}$, then the minimum of any C II $\lambda 6580$ signature would be between 6120 – 6280 \AA . If weak and blue-shifted to these wavelengths, the C II $\lambda 6580$ absorption would most likely go undetected. If the C II optical depth were large enough, then the most direct evidence for hidden C II $\lambda 6580$ would be whether or not an associated absorption from C II $\lambda 7234$ could be seen between 6730 – 6900 \AA .

This raises the question: At what velocity will C II $\lambda 6580$ completely blend with Si II $\lambda 6580$? In Figure 6, we presented observed C II $\lambda 6580$ blending scenarios where the signature is weak and nearly hidden, such as possibly observed in SN 2001V and 2009ig. These objects suggest that C II $\lambda 6580$ absorption features can in some cases be obscured via line blending. Such a “hidden” C II signature would be seen in the form of an absorption on the shoulder on the blue wing of the Si II $\lambda 6355$ emission component.

A series of synthetic spectra that include only blends of Si II $\lambda 6355$ and C II $\lambda 6580$ line profiles are shown in Figure 9 (top panel). For these SYNOW spectra, the velocity of Si II was fixed at $10,000 \text{ km s}^{-1}$ while the velocity of C II was increased from this $10,000 \text{ km s}^{-1}$ by 1000

km s⁻¹ increments up to a velocity of 15,000 km s⁻¹. We simultaneously decreased the optical depth in keeping consistency with the observed profile shapes. At a velocity of 15,000 km s⁻¹, C II λ 6580 loses its discernibility as a feature and remains hidden until C II reaches a velocity of 27,000 km s⁻¹. At present there are no observations reporting a C II λ 6580 feature appearing blue-ward of the Si II λ 6355 absorption.

Aside from being able to account for the observed variety of C II absorption profile shapes and velocities with respect to Si II λ 6355, in Figure 9 we also show that the shoulder effect can be reproduced when C II is detached with a velocity \sim 4000 km s⁻¹ greater than that of Si II. This is consistent with our fit for SN 2001V where we have C II and Si II at 12,000 and 8000 km s⁻¹, respectively.

In Figure 9 (bottom panel), we show a series of synthetic spectra where C II and Si II are placed at the same velocity and increased in sequence from 10,000 to 18,000 km s⁻¹. We modeled the Si II profiles using the two-component method so as to reproduce HVG-like properties. As can be seen, the C II λ 6580 absorption feature can be easily obscured at higher velocities. The proposed weak C II λ 6580 feature for SN 2009ig lies atop the emission component of Si II λ 6355 and is consistent with this series of synthetic spectra.

It is generally thought that the infrequent number of HVGs where C II λ 6580 is detected suggests an environment of sparse carbon-rich regions (Pignata et al. 2008). However, if the proposed C II λ 6580 signature in SN 2009ig is correct, then our fits suggest that the feature could be weak based on line blending, and not necessarily due to a low carbon abundance (or lower than that of LVGs) alone.

6.3. Asymmetries in the Distribution of C II Regions

Because the ejected material follow a homologous expansion law ($v \propto r$), the degree to which electron scattering will polarize emergent light across a spectral line can provide geometrical information on the material between the observer and the photosphere (Shapiro & Sutherland 1982; Wang & Wheeler 2008). Spectropolarimetry of some SNe Ia have revealed that the distribution of the outermost ejected material has an overall deviation from spherical symmetry of up to \sim 10% (Höflich 1991; Wang et al. 1997). Specifically, optical Si II P-Cygni profiles are observed to have peak polarization values of 0.3–2.0%, five days before maximum light (Wang et al. 2007). Other absorption features, such as the Ca II IR triplet, have also been observed to be strongly polarized (Wang et al. 2003; Kasen et al. 2003).

Of the 19 SNe Ia in our sample, only SN 1994D, 1999by and 2005hk have nearly simultaneous spectroscopic and polarization data during the presence of a C II λ 6580 absorption feature. Polarization levels for these objects across Si II λ 6355 were reported as insignificant (\sim 0.3% for SN 1994D, Wang et al. 1996; \sim 0.4% for SN 1999by, Howell et al. 2001; \sim 0.4% for SN 2005hk, Chornock et al. 2006), whereas the degree of polarization was even less in the region of the C II λ 6580 signature.

Regarding SN 1999by, the three spectropolarimetric observations of Howell et al. (2001) were combined from data taken on days -2 , -1 and 0 in order to increase the S/N ratio (see their Fig. 2). The resultant spectrum

exhibited the same 6300 Å absorption feature that was attributed to C II λ 6580 in the day -5 , -4 and -3 spectra of Garnavich et al. (2004), but the concurrent polarimetry data of Howell et al. (2001) did not show any significant amount of polarization near the feature. This would suggest that the C II regions are roughly spherical in at least these objects. However, because spectropolarimetric observations are most useful when a spectral line is strong and the S/N is high, it is difficult to use the weak C II λ 6580 absorption features of SNe Ia to infer asymmetries of carbon-rich regions with polarization data. Despite this, possible asymmetries of carbon-rich regions might be gleaned through other means.

Recently, Maeda et al. (2010b) discussed SN Ia diversity in the context of global asymmetries of ejected material. They argued that the HVG and LVG subtypes constitute a picture of SNe Ia in terms of an off-center delayed-detonation at different viewing angles. In this scenario, an off-center ignition is followed by the propagation of a sub-sonic deflagration flame that imprints an off-set distribution of high density ash. Once the transition to detonation occurs, a super-sonic flame only successfully burns material in the lower density regions and is effectively screened by some of the deflagration ash. What remains is a lopsided distribution of burning products, resulting in a hemispheric asymmetry of the ejecta. Similarly, Maund et al. (2010) reached the same conclusion regarding SN Ia diversity after examining a possible relationship between HVG/LVG subtypes and the possible asymmetrical distribution of photospheric Si II.

In this model, LVGs correspond to viewing the hemisphere of ejecta that coincides with the off-center ignition, whereas HVGs are the contrary with an opening angle of \sim 70–75°. Since we do not see a predominate number of HVGs with conspicuous C II λ 6580 features in our sample, this is consistent with the above model, owing to the fact that detonation waves ought to leave little unburned material behind on the HVG side. If Maeda et al. (2010b) is correct, and if our sample of SN Ia that exhibit C II λ 6580 is representative, then this suggests that the filling factor of carbon in the LVG hemisphere is less than unity.

7. CONCLUSIONS

In an effort to better understand the frequency and general properties of C II absorption features, we examined C II λ 6580 signatures in the pre-maximum spectra of 19 SNe Ia, of which included 14 “normal” SNe Ia, three possible Super-Chandra SNe Ia, and two 2002cx-like events. Using SYNOW to produce synthetic spectra, we modeled observed \sim 6300 Å absorption features as a C II λ 6580 P-Cygni profile blended with that of Si II λ 6355. Through our SYNOW model fits we estimated the C II expansion velocities for a variety of objects. Below is a summary of our major findings:

1. A survey of the optical spectra of 68 objects published in the literature since 1983 January 1 indicates that up to \sim 30% of SNe Ia display an absorption feature near 6300 Å that can be attributed to C II λ 6580. While this percentage is likely biased, it does suggest that C II λ 6580 absorption features are more common than was previously suspected (Thomas et al. 2007). If spectroscopic observations

of SNe Ia are obtained more than ~ 1 week before maximum light, we suspect an even larger fraction of SNe Ia of all subtypes may show identifiable C II absorption signatures.

2. A greater frequency of C II $\lambda 6580$ absorption features appear in the low-velocity gradient subtypes (LVGs) compared to high-velocity gradient events (HVGs). This is in line with the interpretation of Maeda et al. (2010b), supporting the idea that part of SN Ia diversity can be accounted for by viewing angle and off-center ignition effects.
3. The influence of the temperature of the carbon-rich region on the incidence of C II $\lambda 6580$ signatures is most evident for the 14 “normal” SNe Ia in our survey. The frequency of C II $\lambda 6580$ signatures peaks with the Core-Normal (CN) SNe Ia, while the Cool (CL) and Shallow-Silicon (SS) subtypes exhibit fewer C II $\lambda 6580$ detections. This result is consistent with the effective temperature sequence of Nugent et al. (1995).
4. We find the values of $v(\text{C II } \lambda 6580)/v(\text{Si II } \lambda 6355)$ among 16 of the SNe Ia in our C II sample are similar to within $\pm 10\%$. Assuming the minima of Si II $\lambda 6355$ absorption features are an appropriate measure of photospheric velocities prior to maximum light, then the small number of cases where $v(\text{C II } \lambda 6580)/v(\text{Si II } \lambda 6355) < 1$ could be indicative of either a layered distribution or multiple clumps with a comparable filling factor.

One of the most interesting results of this study is that C II $\lambda 6580$ absorption features might be in many, if not most, early-epoch SN Ia spectra. We initially set out to investigate what we suspected was a small number of known detections of C II $\lambda 6580$. However, when we examined the 6300 Å region in a relatively large sample of objects, we discovered that weak signatures of C II $\lambda 6580$ were often detectable and could influence the observed Si II $\lambda 6355$ spectral profile.

One way to test for a high frequency of C II $\lambda 6580$ features in pre-maximum SNe Ia spectra would be to obtain high S/N observations of the region between 6700–7200 Å in order to look for the relatively weaker C II $\lambda 7234$ line that should also be present. In addition, a data set of C II $\lambda 6580$ observations with wavelength coverage that encompasses the O I $\lambda 7774$ absorption feature would allow for investigating any correlations between C and O spectral line properties.

Understanding the presence of C II in SN Ia spectra may prove to be a valuable diagnostic of SN Ia diversity and therefore a possible means by which to probe the underlying explosion mechanism. Utilizing the absolute strength of the C II $\lambda 6580$ line in order to extract abundance information will require comparison to synthetic spectra calculations based on hydrodynamical modeling. A detailed comparative study that can extract C abundance information, derived from C II $\lambda 6580$ absorption features, promises to produce a wealth of insight regarding carbon-rich regions, and therefore constrain the parameter space of hydrodynamical modeling.

We are grateful to Laura Kay for obtaining some of the spectra of SN 2010Y and thank Eddie Baron, David Branch, and Andy Howell for helpful comments on an earlier draft of this paper. J.V. has received support from NSF Grant AST-0707669, Texas Advanced Research Program grant ASTRO-ARP-0094 and Hungarian OTKA Grant K76816.

REFERENCES

- Aldering, G., et al. 2002, Proc. SPIE, 4836, 61
 Arnett, W. D. 1969, Ap&SS, 5, 180
 Arnett, W. D. 1982, ApJ, 253, 785
 Aspden, A. J., Bell, J. B., & Woosley, S. E. 2010, ApJ, 710, 1654
 Barbon, R., Rosino, L., & Iijima, T. 1989, A&A, 220, 83
 Baron, E., Hauschildt, P. H., & Branch, D. 1994, ApJ, 426, 334
 Baron, E., Lentz, E. J., & Hauschildt, P. H. 2003, ApJ, 588, L29
 Baron, E., Chen, B., & Hauschildt, P. H. 2009, American Institute of Physics Conference Series, 1171, 148
 Benetti, S., et al. 2005, ApJ, 623, 1011
 Blondin, S., & Tonry, J. L. 2007, ApJ, 666, 1024
 Bongard, S., Baron, E., Smadja, G., Branch, D., & Hauschildt, P. H. 2008, ApJ, 687, 456
 Branch, D., Lacy, C. H., McCall, M. L., Sutherland, P. G., Uomoto, A., Wheeler, J. C., & Wills, B. J. 1983, ApJ, 270, 123
 Branch, D., & Khokhlov, A. M. 1995, Phys. Rep., 256, 53
 Branch, D., et al. 2003, AJ, 126, 1489
 Branch, D., Baron, E., Hall, N., Melakayil, M., & Parrent, J. 2005, PASP, 117, 545
 Branch, D., et al. 2006, PASP, 118, 560
 Branch, D., Parrent, J., Troxel, M. A., Casebeer, D., Jeffery, D. J., Baron, E., Ketchum, W., & Hall, N. 2007, AIP Conference Proceedings, 924, 342
 Branch, D., et al. 2008, PASP, 120, 135
 Branch, D., Dang, L. C., & Baron, E. 2009, PASP, 121, 238
 Chen, W.-C., & Li, X.-D. 2009, ApJ, 702, 686
 Chornock, R., Filippenko, A. V., Branch, D., Foley, R. J., Jha, S., & Li, W. 2006, PASP, 118, 722
 Colgate, S. A., & McKee, C. 1969, ApJ, 157, 623
 Elias, J. H., Matthews, K., Neugebauer, G., & Persson, S. E. 1985, ApJ, 296, 379
 Elias-Rosa, N., et al. 2006, MNRAS, 369, 1880
 Filippenko, A. V. 1997, ARA&A, 35, 309
 Fisher, A., Branch, D., Nugent, P., & Baron, E. 1997, ApJ, 481, L89
 Fisher, A., Branch, D., Hatano, K., & Baron, E. 1999, MNRAS, 304, 67
 Foley, R. J., et al. 2009, AJ, 138, 376
 Foley, R. J., Brown, P. J., Rest, A., Challis, P. J., Kirshner, R. P., & Wood-Vasey, W. M. 2010, ApJ, 708, L61
 Foley, R. J., Narayan, G., Challis, P. J., Filippenko, A. V., Kirshner, R. P., Silverman, J. M., & Steele, T. N. 2010, ApJ, 708, 1748
 Gamezo, V. N., Khokhlov, A. M., & Oran, E. S. 2004, Physical Review Letters, 92, 211102
 Gamezo, V. N., Khokhlov, A. M., & Oran, E. S. 2005, ApJ, 623, 337
 Garavini, G., et al. 2004, AJ, 128, 387
 Garavini, G., et al. 2005, AJ, 130, 2278
 Garnavich, P. M., et al. 2004, ApJ, 613, 1120
 Harutyunyan, A., Benetti, S., Cappellaro, E., & Turatto, M. 2005, 1604-2004: Supernovae as Cosmological Lighthouses, 342, 258
 Harutyunyan, A. H., et al. 2008, A&A, 488, 383
 Hatano, K., Branch, D., Fisher, A., Baron, E., & Filippenko, A. V. 1999, ApJ, 525, 881
 Hatano, K., Branch, D., Fisher, A., Millard, J., & Baron, E. 1999, ApJS, 121, 233
 Hatano, K., Branch, D., Qiu, Y. L., Baron, E., Thielemann, F.-K., & Fisher, A. 2002, New Astronomy, 7, 441
 Hernandez, M., et al. 2000, MNRAS, 319, 223 & Fisher, A. 2002, New Astronomy, 7, 441
 Hicken, M., Garnavich, P. M., Prieto, J. L., Blondin, S., DePoy, D. L., Kirshner, R. P., & Parrent, J. 2007, ApJ, 669, L17
 Hill, G. J., et al. 1998, Proc. SPIE, 3355, 375
 Höflich, P. 1990, A&A, 229, 191

- Höflich, P. 1991, *A&A*, 246, 481
- Höflich, P., Khokhlov, A. M., & Wheeler, J. C. 1995, *ApJ*, 444, 831
- Höflich, P., Gerardy, C. L., Fesen, R. A., & Sakai, S. 2002, *ApJ*, 568, 791
- Howell, D. A., Höflich, P., Wang, L., & Wheeler, J. C. 2001, *ApJ*, 556, 302
- Howell, D. A., et al. 2005, *ApJ*, 634, 1190
- Howell, D. A., et al. 2006, *Nature*, 443, 308
- Howell, D. A. 2010, arXiv:1011.0441
- Hoyle, F., & Fowler, W. A. 1960, *ApJ*, 132, 565
- Iben, I., Jr. 1988, *ApJ*, 324, 355
- Jeffery, D. J., & Branch, D. 1990, *Supernovae, Jerusalem Winter School for Theoretical Physics*, 149
- Jeffery, D. J., Ketchum, W., Branch, D., Baron, E., Elmhamdi, A., & Danziger, I. J. 2007, *ApJS*, 171, 493
- Kasen, D., et al. 2003, *ApJ*, 593, 788
- Kasen, D., Thomas, R. C., Röpke, F., & Woosley, S. E. 2008, *Journal of Physics Conference Series*, 125, 012007
- Kasen, D., Röpke, F. K., & Woosley, S. E. 2009, *Nature*, 460, 869
- Khokhlov, A. M. 1991, *A&A*, 245, 114
- Kirshner, R. P., et al. 1993, *ApJ*, 415, 589
- Kotak, R., et al. 2005, *A&A*, 436, 1021
- Kozma, C., Fransson, C., Hillebrandt, W., Travaglio, C., Sollerman, J., Reinecke, M., Röpke, F. K., & Spyromilio, J. 2005, *A&A*, 437, 983
- Lentz, E. J., Baron, E., Branch, D., & Hauschildt, P. H. 2001, *ApJ*, 557, 266
- Leonard, D. C., Li, W., Filippenko, A. V., Foley, R. J., & Chornock, R. 2005, *ApJ*, 632, 450
- Li, W. D., et al. 1999, *AJ*, 117, 2709
- Li, W., et al. 2001, *PASP*, 113, 1178
- Li, W., et al. 2003, *PASP*, 115, 453
- Maeda, K., Röpke, F. K., Fink, M., Hillebrandt, W., Travaglio, C., & Thielemann, F.-K. 2010, *ApJ*, 712, 624
- Maeda, K., et al. 2010, *Nature*, 466, 82
- Marion, G. H., Höflich, P., Wheeler, J. C., Robinson, E. L., Gerardy, C. L., & Vacca, W. D. 2006, *ApJ*, 645, 1392
- Marion, G. H., Höflich, P., Gerardy, C. L., Vacca, W. D., Wheeler, J. C., & Robinson, E. L. 2009, *AJ*, 138, 727
- Marion, et al. 2011, in preparation
- Matheson, T., et al. 2008, *AJ*, 135, 1598
- Mattila, S., Lundqvist, P., Sollerman, J., Kozma, C., Baron, E., Fransson, C., Leibundgut, B., & Nomoto, K. 2005, *A&A*, 443, 649
- Maund, J. R., et al. 2010, *ApJ*, 725, L167
- Mazzali, P. A. 2000, *A&A*, 363, 705
- Mazzali, P. A. 2001, *MNRAS*, 321, 341
- Mazzali, P. A., Benetti, S., Stehle, M., Branch, D., Deng, J., Maeda, K., Nomoto, K., & Hamuy, M. 2005, *MNRAS*, 357, 200
- McClelland, C. M., et al. 2010, *ApJ*, 720, 704
- Niemeyer, J. C. 1998, *Stellar Evolution, Stellar Explosions and Galactic Chemical Evolution*, 673
- Nomoto, K., Thielemann, F.-K., & Yokoi, K. 1984, *ApJ*, 286, 644
- Nomoto, K., Uenishi, T., Kobayashi, C., Umeda, H., Ohkubo, T., Hachisu, I., & Kato, M. 2003, *From Twilight to Highlight: The Physics of Supernovae*, 115
- Nugent, P., Phillips, M., Baron, E., Branch, D., & Hauschildt, P. 1995, *ApJ*, 455, L147
- Nugent, P., Sullivan, M., & Howell, D. A. 2010, *The Astronomer's Telegram*, 2657, 1
- Pastorello, A., et al. 2007, *MNRAS*, 377, 1531
- Patat, F., Benetti, S., Cappellaro, E., Danziger, I. J., della Valle, M., Mazzali, P. A., & Turatto, M. 1996, *MNRAS*, 278, 111
- Phillips, M. M., et al. 1987, *PASP*, 99, 592
- Phillips, M. M. 1993, *ApJ*, 413, L105
- Pignata, G., et al. 2008, *MNRAS*, 388, 971
- Pope, S., B. 1987, *Annual Rev. Fluid Mech.*, 19, 237
- Poznanski, D., et al. 2010, *Science*, 327, 58
- Prieto, J. L., et al. 2007, arXiv:0706.4088
- Quimby, R., Höflich, P., Kannappan, S. J., Rykoff, E., Rujopakarn, W., Akerlof, C. W., Gerardy, C. L., & Wheeler, J. C. 2006, *ApJ*, 636, 400
- Quimby, R., Höflich, P., & Wheeler, J. C. 2007, *ApJ*, 666, 1083
- Ramsey, L. W., et al. 1998, *Proc. SPIE*, 3352, 34
- Rau, A., et al. 2009, *PASP*, 121, 1334
- Röpke, F. K. 2005, *A&A*, 432, 969
- Sadakane, K., et al. 1996, *PASJ*, 48, 51
- Sahu, D. K., et al. 2008, *ApJ*, 680, 580
- Salvo, M. E., Cappellaro, E., Mazzali, P. A., Benetti, S., Danziger, I. J., Patat, F., & Turatto, M. 2001, *MNRAS*, 321, 254
- Scalzo, R. A., et al. 2010, arXiv:1003.2217
- Shapiro, P. R., & Sutherland, P. G. 1982, *ApJ*, 263, 902
- Sobolev, V. V. 1957, *Soviet Astronomy*, 1, 678 1009
- Stanishev, V., et al. 2007, *A&A*, 469, 645
- Stehle, M., Mazzali, P. A., Benetti, S., & Hillebrandt, W. 2005, *MNRAS*, 360, 1231
- Tanaka, M., et al. 2008, *ApJ*, 677, 448
- Tanaka, M., et al. 2010, *ApJ*, 714, 1209
- Tanaka, M., Mazzali, P. A., Stanishev, V., Maurer, I., Kerzendorf, W. E., & Nomoto, K. 2011, *MNRAS*, 410, 1725
- Taubenberger, S., et al. 2008, *MNRAS*, 385, 75
- Taubenberger, S., et al. 2011, *MNRAS*, 61
- Thielemann, F.-K., Nomoto, K., & Yokoi, K. 1986, *A&A*, 158, 17
- Thomas, R. C., Kasen, D., Branch, D., & Baron, E. 2002, *ApJ*, 567, 1037
- Thomas, R. C., et al. 2007, *ApJ*, 654, L53
- Travaglio, C., Hillebrandt, W., Reinecke, M., & Thielemann, F.-K. 2004, *A&A*, 425, 1029
- Turatto, M., Benetti, S., Cappellaro, E., Danziger, I. J., Della Valle, M., Gouiffes, C., Mazzali, P. A., & Patat, F. 1996, *MNRAS*, 283, 1
- Turatto, M., Piemonte, A., Benetti, S., Cappellaro, E., Mazzali, P. A., Danziger, I. J., & Patat, F. 1998, *AJ*, 116, 2431
- Valenti, S., et al. 2009, *Nature*, 459, 674
- Valentini, G., et al. 2003, *ApJ*, 595, 779
- Wang, L., Wheeler, J. C., Li, Z., & Clocchiatti, A. 1996, *ApJ*, 467, 435
- Wang, L., Wheeler, J. C., & Höflich, P. 1997, *ApJ*, 476, L27
- Wang, L., et al. 2003, *ApJ*, 591, 1110
- Wang, L., Baade, D., Höflich, P., Wheeler, J. C., Kawabata, K., Khokhlov, A., Nomoto, K., & Patat, F. 2006, *ApJ*, 653, 490
- Wang, L., Baade, D., & Patat, F. 2007, *Science*, 315, 212
- Wang, L., & Wheeler, J. C. 2008, *ARA&A*, 46, 433
- Wang, X., et al. 2009, *ApJ*, 697, 380
- Wells, L. A., et al. 1994, *AJ*, 108, 2233
- Woosley, S. E., Kerstein, A. R., Sankaran, V., Aspden, A. J., Röpke, F. K. 2009, *ApJ*, 704, 255
- Yamanaka, M., et al. 2009, *PASJ*, 61, 713
- Yamanaka, M., et al. 2009, *ApJ*, 707, L118
- Zhang, T., et al. 2010, *PASP*, 122, 1

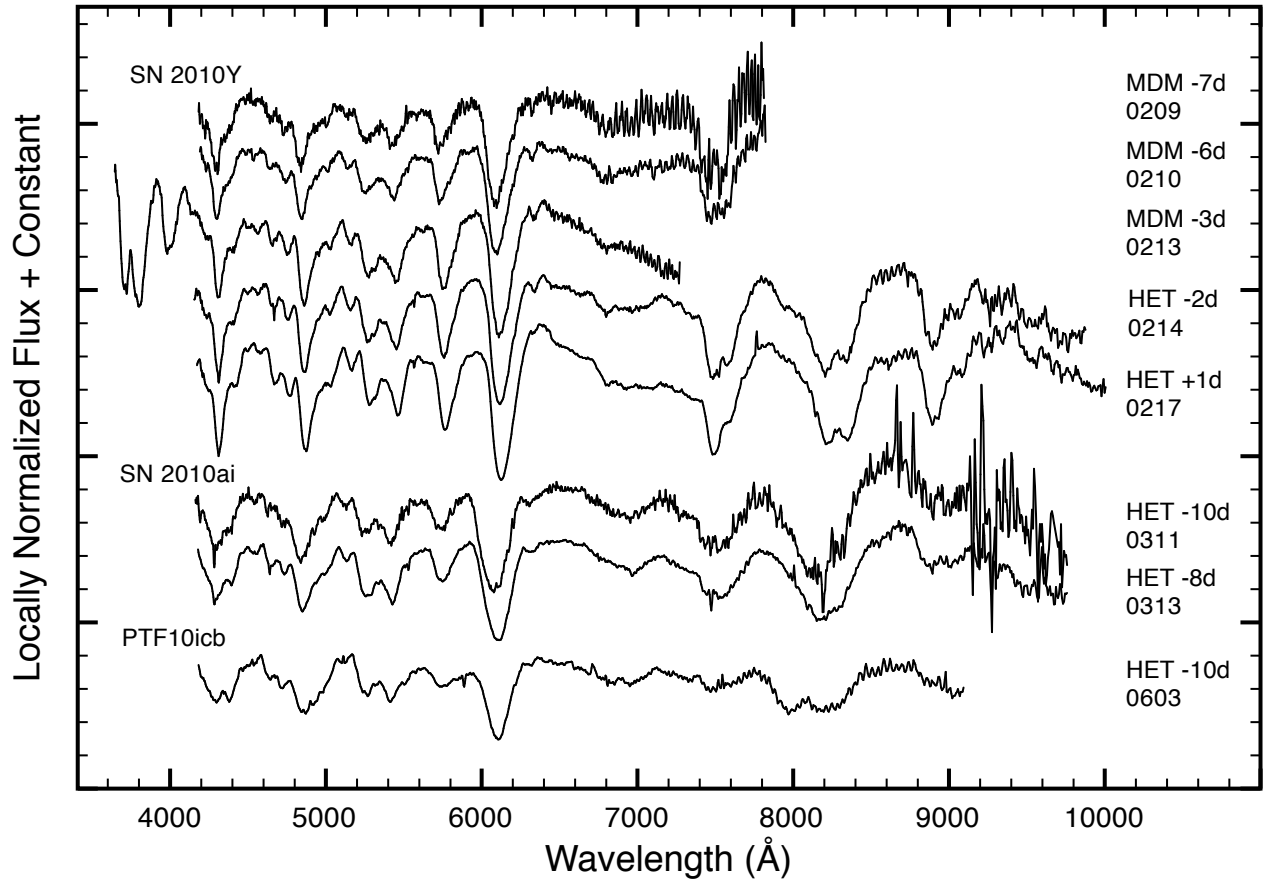


Figure 1. Pre-maximum spectra of SN 2010Y, 2010ai, and PTF10icb. Data are from HET and the 2.4 m Hiltner at MDM, have been scaled appropriately, and are in the rest frame of their respective host galaxy. Absorption features that are consistent with C II $\lambda 6580$ blue-shifted to typical expansion velocities of SNe Ia are seen at ~ 6300 Å. See Table 2 for observational details.

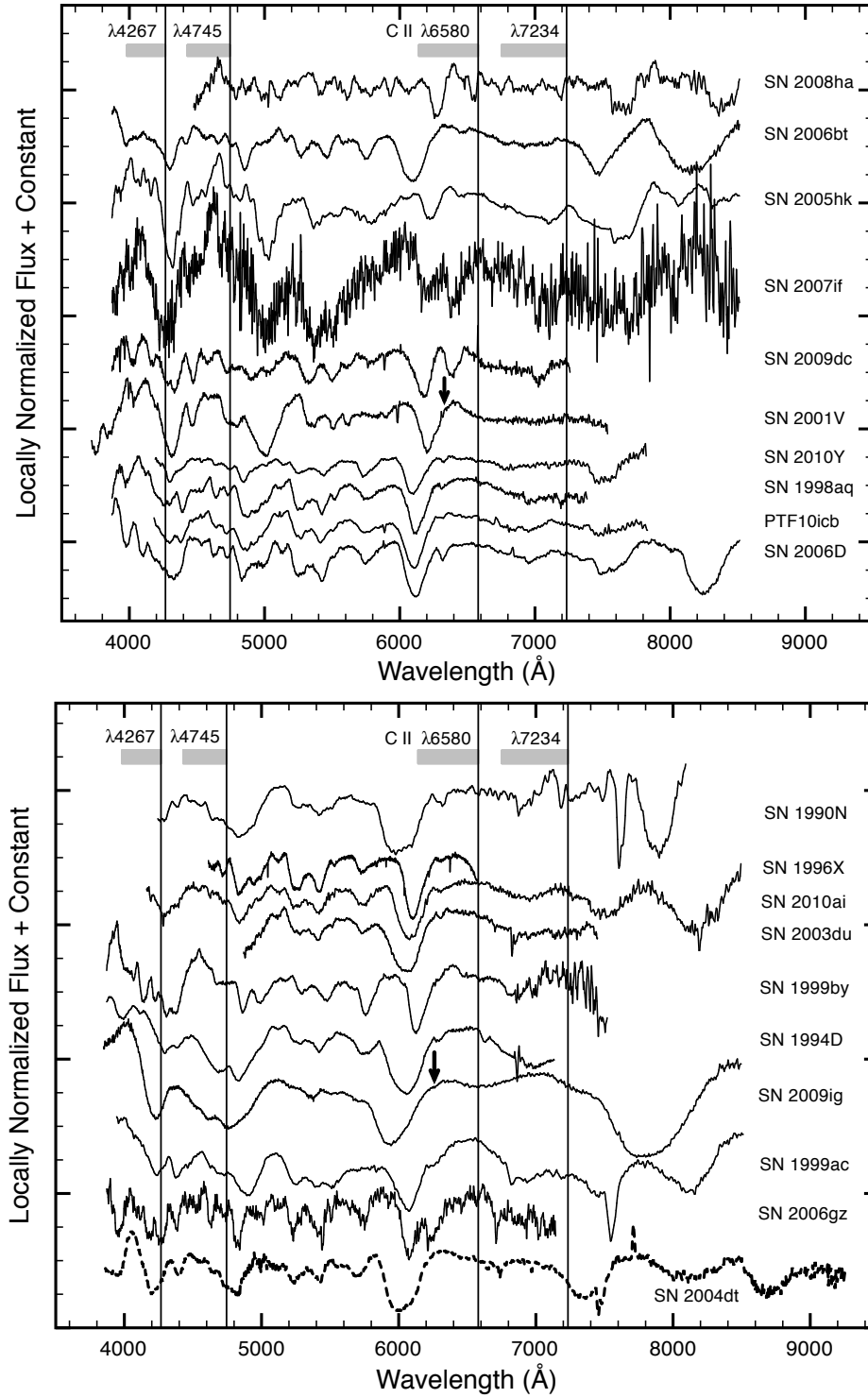


Figure 2. Sample of 19 SNe Ia whose pre-maximum optical spectra contain an absorption due to C II $\lambda 6580$. A pre-maximum spectrum of SN 2004dt (HVG) is shown at the bottom (dashed line) for comparison. Spectra have been normalized and corrected for host galaxy redshift. Vertical lines indicate the rest wavelength position of C II $\lambda\lambda 4267, 4745, 6580, \text{ and } 7234$. The width of the shaded regions near each vertical line corresponds to Doppler velocities between $1000 - 20,000 \text{ km s}^{-1}$. To guide the eye, a couple black arrows indicate the position of a likely absorption feature of C II $\lambda 6580$.

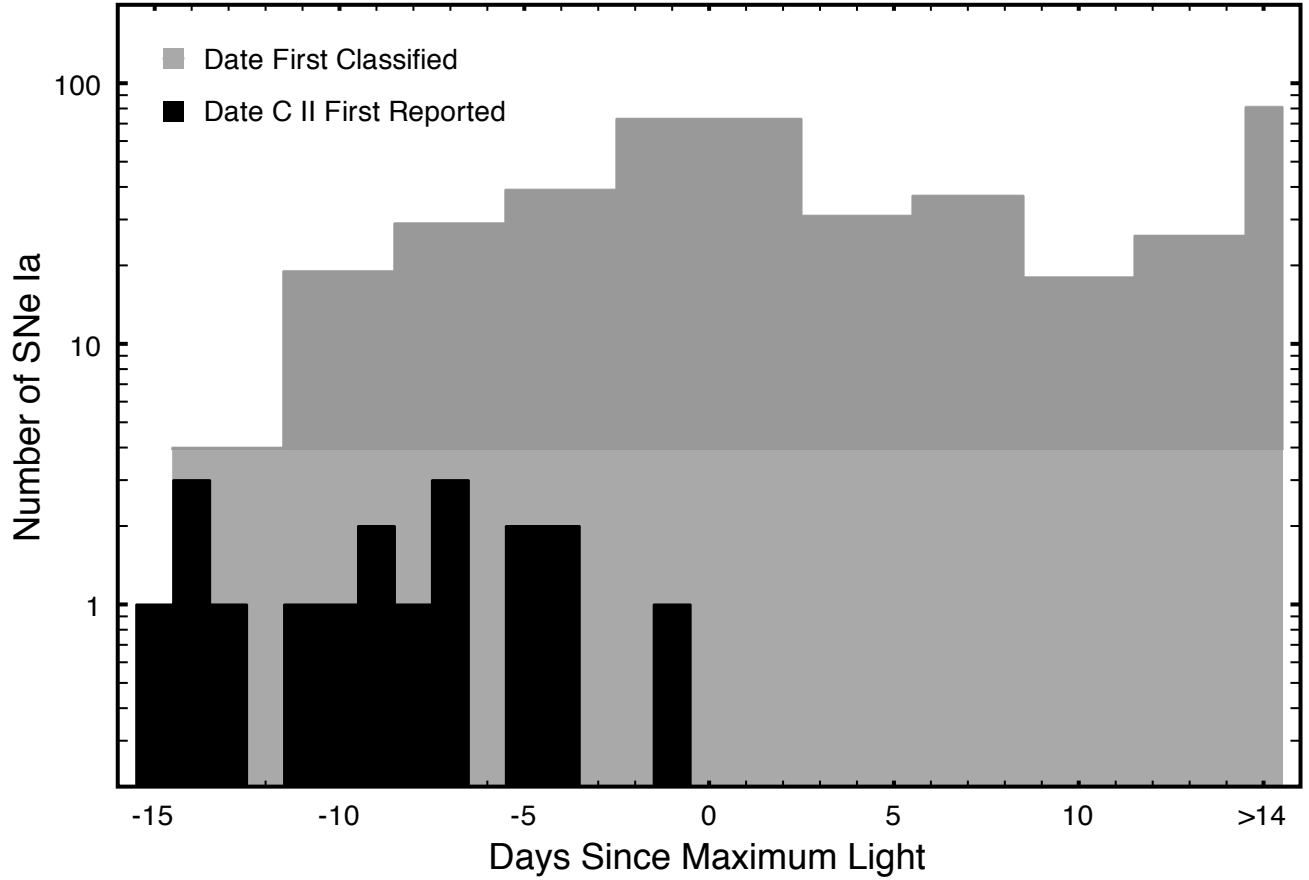


Figure 3. Shaded in grey are the number of SNe Ia discovered between 2006 January 1 and 2009 December 1 plotted against the epoch at which they were identified as being a Type Ia supernovae. Shaded in black are the number of SNe Ia that show ~ 6300 absorption features in their pre-maximum spectra at the time when the feature was first seen. Data were taken from Central Bureau Electronic Telegrams (CBET) and Astronomical Telegrams (ATEL). Estimates for the age of each supernova were obtained by one of several publicly available spectrum-comparison tools (PASSparToo; Harutyunyan et al. (2005), Superfit; Howell et al. (2005), SNID; Blondin & Tonry (2007), GELATO; Harutyunyan et al. (2008)). The cited epoch for each SNe Ia in this plot was taken as reported in the telegrams. The numbers above are not a strict sampling of all objects during the four year period, given that some of the age estimates were too vague to be included. This explains the peaks at day -7 , 0 , $+7$ and $+14$ relative to maximum light. Because the spectral identification programs determine age with several days of error, we binned the data sample at days -13 ± 1 , -10 ± 1 , -7 ± 1 , -4 ± 1 , 0 ± 2 , $+4 \pm 1$, $+7 \pm 1$, $+10 \pm 1$ and $+13 \pm 1$. Both histograms show, on average, that observations before 1-week pre-maximum are not well represented compared to observations near maximum light or later.

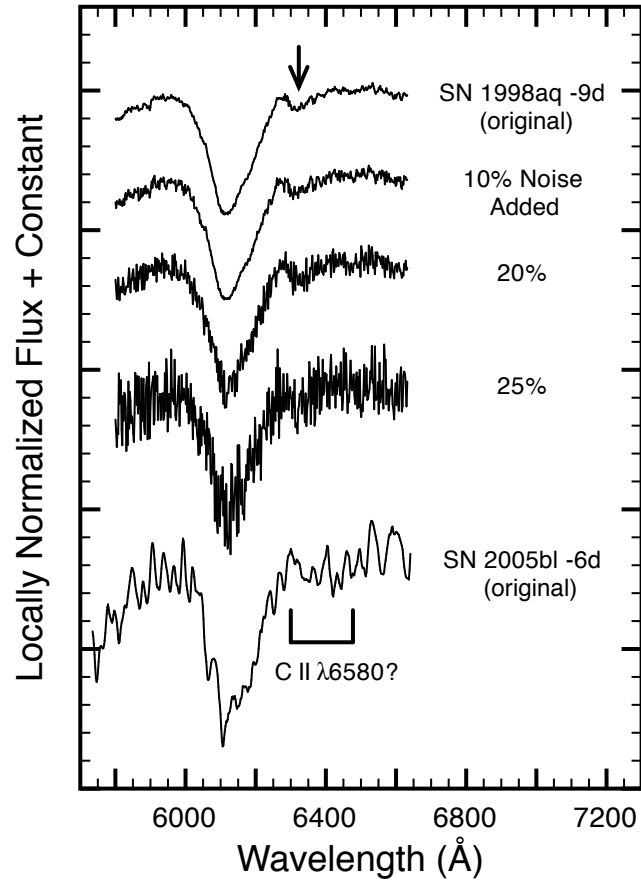


Figure 4. Five segments of spectra showing the questionable of a C II $\lambda 6580$ absorption feature as a function of the signal-to-noise ratio. At the top is the original spectrum for the day -9 observation of SN 1998aq. The three spectra that follow represent the day -9 spectrum with 10, 20, and 25% Gaussian noise added. The spectrum at the bottom is that of SN 2005bl, six days before maximum light, where Taubenberger et al. (2008) identified the 6400 Å feature with that of C II $\lambda 6580$.

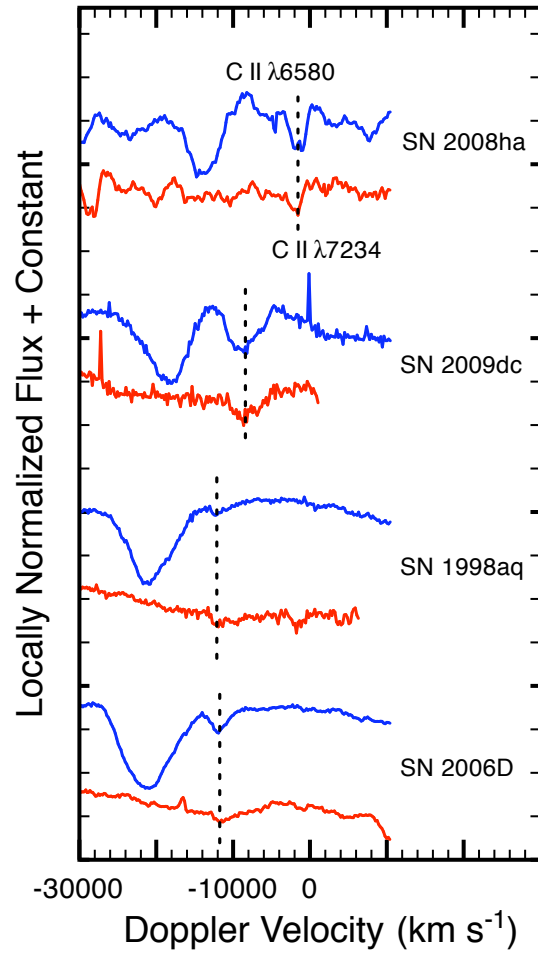


Figure 5. Doppler velocity scaled spectra for four of the SNe Ia in our sample. Blue and red lines represent C II $\lambda 6580$, $\lambda 7234$, respectively, for each SN. Dashed vertical lines are positioned at the minima of the absorption features to guide the eye.

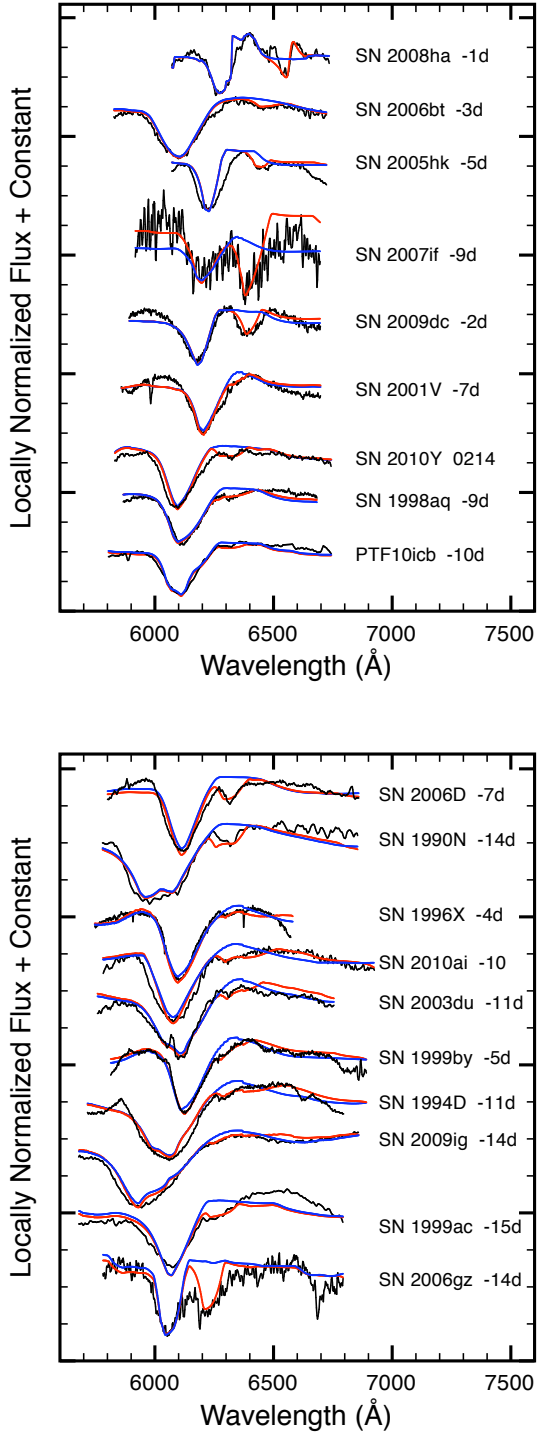


Figure 6. SYNOW fits of the 19 SNe Ia in our sample presented in two panels. The red and blue lines denote a synthetic fit to the spectrum of a SNe Ia with and without C II, respectively. The contrast between both fits suggests the presence of C II with varying strength in these objects. See Table 2 for fitting parameters.

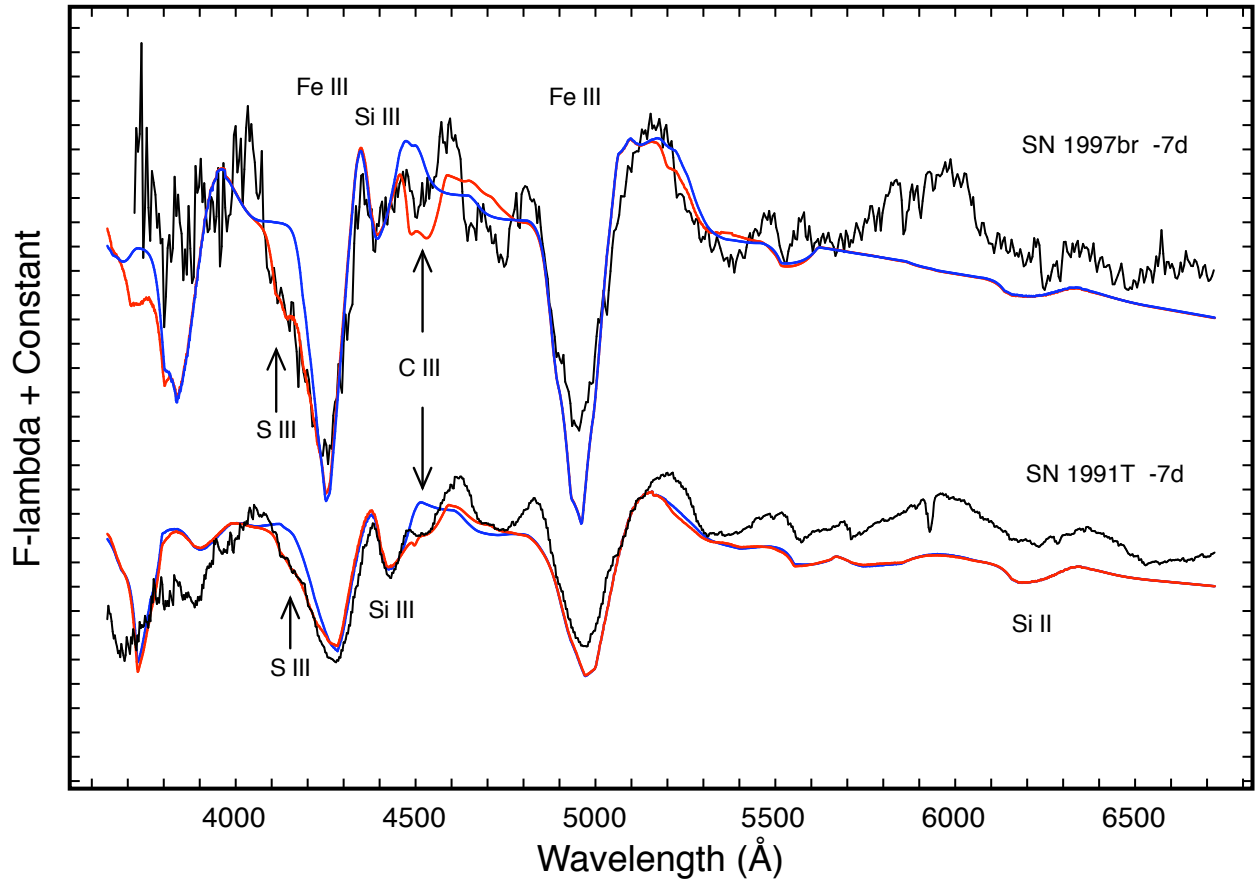


Figure 7. SYNOW fits for SN 1991T and 1997br, two SS SNe Ia, around 1-week pre-maximum. In addition to matching the major features with Fe III, S II, Si II, and Si III, the absorption at 4500 Å is identified with a multiplet of C III λ 4649. As before in Figure 6, the red line denotes the synthetic spectrum with carbon, and the blue line is without.

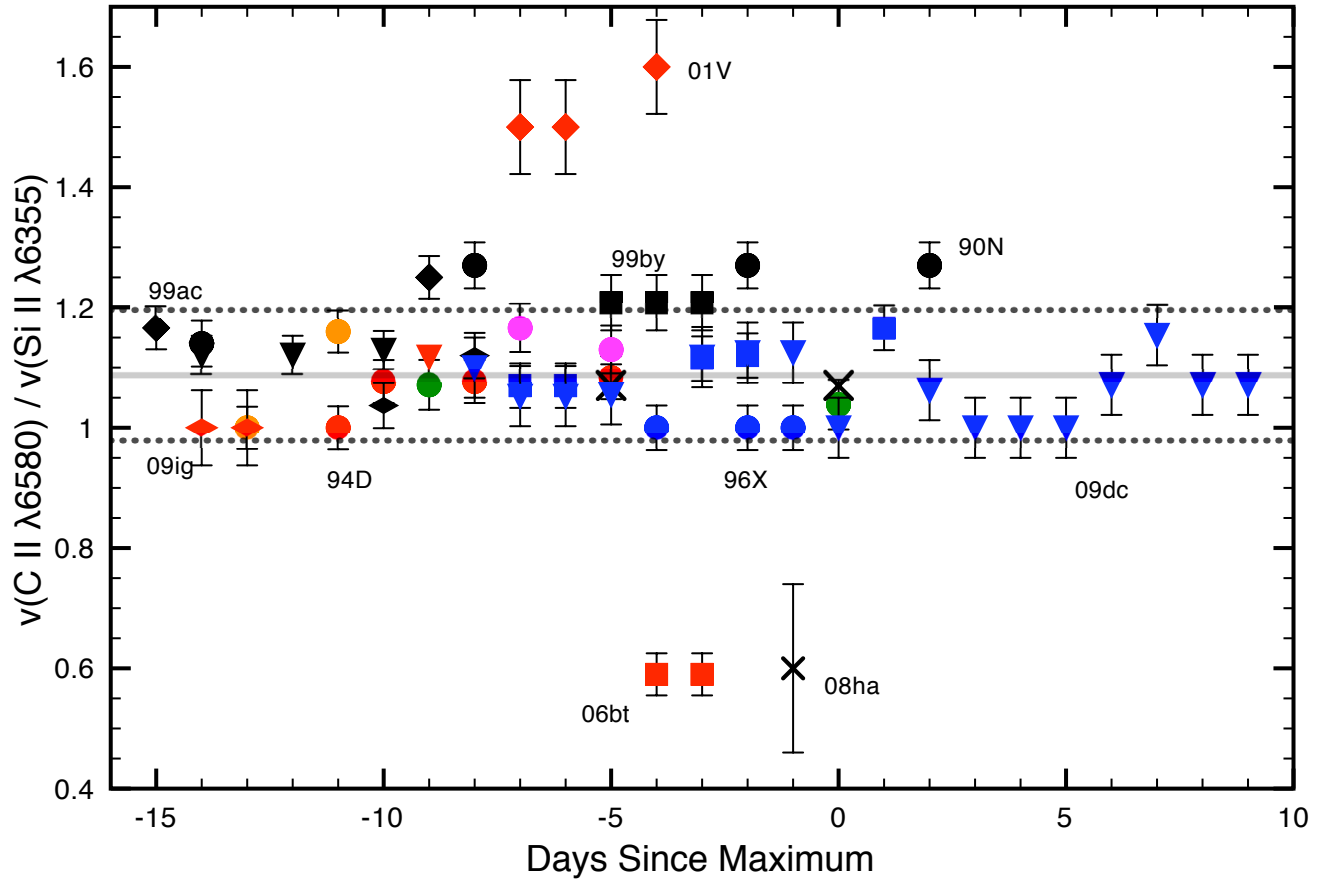


Figure 8. $v(\text{C II } \lambda 6580)/v(\text{Si II } \lambda 6355)$ vs. epoch for our C II–SNe sample. Circles show CNe, side-ways diamonds show BLs, squares show CLs, diamonds show SSs, upside down triangles show Super-Chandra candidates, and the ‘X’ denotes the 2002cx-like, SN 2008ha. Calculated error assumes spectral fits to the velocity of an ion are good to within 500 km s^{-1} . The black horizontal line represents the average value of data points (excluding SN 2001V, 2006bt and 2008ha) and the dashed horizontal lines indicate a 10% difference from the mean.

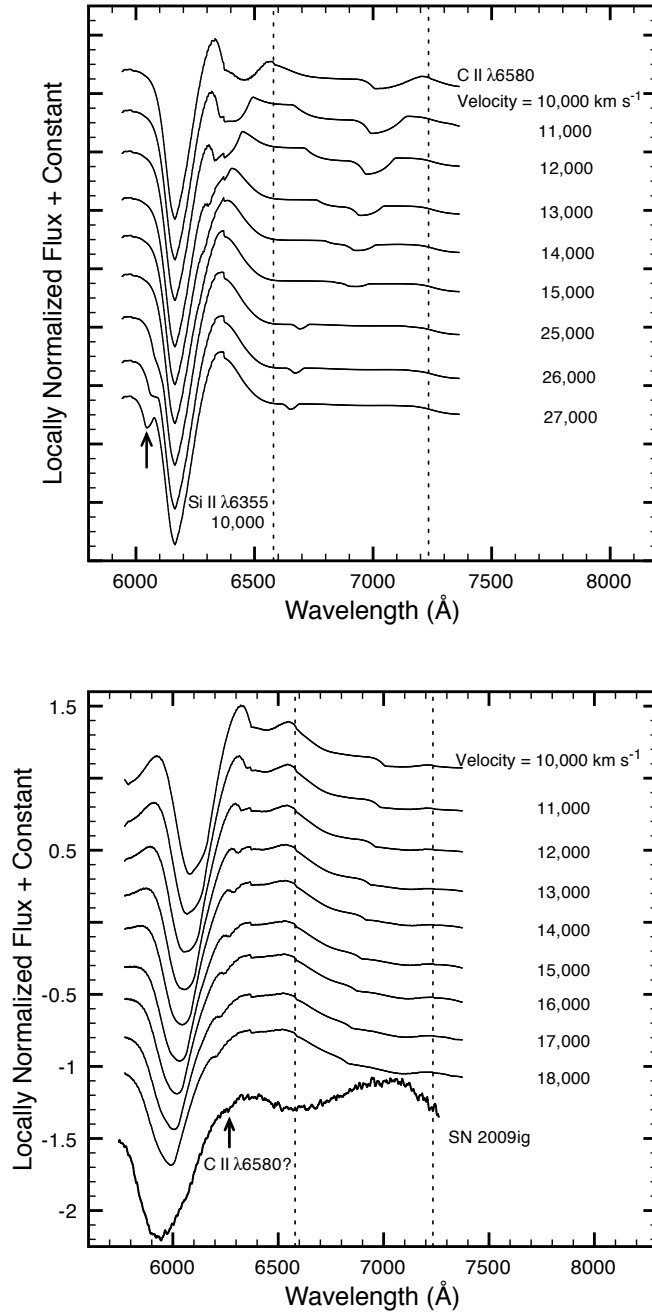


Figure 9. (top) A series of synthetic spectra show an evolution of blending scenarios between C II $\lambda 6580$ and Si II $\lambda 6355$ as the velocity of C II is increased from $10,000$ to $15,000$ km s^{-1} . The two spectra at the bottom represent a case where the C II is present at high velocities. Note that even if the 6580-line is obscured, the 7234-line is blueshifted to the rest frame position of the 6580-line. Three high-velocity scenarios are also shown to note the velocity at which C II $\lambda 6580$ emerges from the blue wing of Si II $\lambda 6355$. (bottom) Like the top figure, but instead C II and Si II are at the same velocity and increased in sequence together while holding τ fixed. The Si II profiles are made from two-components of Si separated by 4000 km s^{-1} . The day -14 spectrum of SN 2009ig is shown for comparison.

Table 1
Summary of Observations

Supernova Name	Host Galaxy	Redshift (km s ⁻¹)	Observation Date	Epoch (days)	Telescope Instrument
SN 2010Y	NGC 3392	3256	2010 Feb 09	-7	MDM/CCDS
			2010 Feb 10	-6	MDM/CCDS
			2010 Feb 13	-3	MDM/CCDS
			2010 Feb 14	-2	HET/LRS
			2010 Feb 17	+1	HET/LRS
SN 2010ai	SDSS J125925.04+275948.2	5507	2010 Mar 11	-10	HET/LRS
			2010 Mar 13	-8	HET/LRS
PTF10icb	2010 June 3	-10	HET/LRS

Table 2
SN Ia Sample

SN Name	Sub-type ^a	C II?	Epoch (days)	Spectrum Source ^e	SN Name	Sub-type	C II?	Epoch (days)	Spectrum Source
LVG									
SN 1990N ^b	CN	Definite	-14	M01	SN 1999dq	SS	No	-9.5	M08
SN 1991T ^b	SS	Possible	-13	F99	SN 1999ee	SS	Uncertain	-9	Mazz05
SN 1994D ^{b,c}	CN	Probable	-11	P96	SN 1999gp	SS	No	-4.5	M08
SN 1995D	CN	Uncertain	+0	S96	SN 2000E	SS	Possible	-6	V03
SN 1996X ^{b,c}	CN	Probable	-4	S01	SN 2001V ^b	SS	Possible	-7	M08
SN 1997br ^b	SS	No	-9	L99	SN 2001el	CN	Probable	-9	Matt05
SN 1997dt	CN	Uncertain	-10	M08	SN 2003cg	CN	Possible	-8.5	E-R06
SN 1998V	CN	Uncertain	+0.5	M08	SN 2003du ^{b,c}	CN	Probable	-11	S07
SN 1998ab	SS	No	-7.5	M08	SN 2005cf	CN	Uncertain	-12	W09
SN 1998aq ^b	CN	Probable	-9	B03	SN 2005cg	SS	No	-10	Q06
SN 1998bu	CN	Probable	-7	H00	SN 2005hj	SS	No	-6	Q07
SN 1998es	SS	No	-10	M08	SN 2006D	CN	Definite	-7	T07
SN 1999aa	SS	No	-11	Gara04	SN 2010ai	CN	Probable	-10	this work
SN 1999ac ^b	SS	Possible	-15	Gara05	PTF10icb	CN	Probable	-10	this work
HVG									
SN 1981B	BL	No	0	B83	SN 2000fa	BL	Uncertain	-10	M08
SN 1984A	BL	No	-7	B89	SN 2002bo	BL	No	-13	S05
SN 1992A	BL	Probable	-6.5	K93	SN 2002dj	BL	No	-11	P08
SN 1997do	BL	No	-11	M08	SN 2002er	BL	Possible	-11	K05
SN 1998dh	BL	No	-9	M08	SN 2004dt ^b	BL	No	-7	W06
SN 1998ec	BL	No	-2.5	M08	SN 2006X	BL	Possible	-7	Y09
SN 1999cc	BL	No	-3	M08	SN 2007gi	BL	Possible	-7.5	Z10
SN 1999cl	BL	No	-7.5	M08	SN 2009ig	BL	Possible	-14	M11, in prep.
SN 1999ej	BL	No	-0.5	M08					
FAINT									
SN 1986G	CL	Possible	-6	P87	SN 2000cn	CL	Uncertain	-9	M08
SN 1989B	CL	Possible	-7	W94	SN 2000dk	CL	Possible	-4.5	M08
SN 1991bg	CL	No	+1	T96	SN 2004eo	CL	No	-11	P07
SN 1997cn	CL	No	0	T98	SN 2005bl ^b	CL	Probable	-6	T08
SN 1998bp	CL	No	-2.5	M08	SN 2006bt	CL	Probable	-3	F10b
SN 1998de	CL	No	-6.5	M08	SN 2010Y	CL	Definite	-7	this work
SN 1999by ^{b,c}	CL	Possible	-5	Gara04					
SC ^d									
SN 2003fg	...	Definite		H06	SN 2006gz ^b	...	Definite	-14	H07
SN 2007if	...	Definite	-9	S10	SN 2009dc	...	Definite	-8	unpublished
misc.									
SN 2000cx	...	Possible	-3	L01	SN 2005hk ^{b,c}	...	Possible	-5	S08
SN 2002bj	...	Definite	+7	P10	SN 2007qd	...	Possible	+3	M10
SN 2002cx	...	Probable	-4	L03	SN 2008ha	...	Definite	-1	F09, F10a

^a SN type notation of Branch et al. (2006), where CN = ‘core normal’, SS = ‘shallow silicon’, CL = ‘cool’, and BL = ‘broad line’. The similar subtypes of Benetti et al. (2005) have been used to separate to these SNe Ia into subclasses.

^b Taken from The Supernova Spectrum Archive, SuSpect.

^c Objects with both published spectropolarimetry data and C II λ 6580 absorption signatures: 1994D; Wang et al. (1996), 1996X; Wang et al. (1997), 1999by; Howell et al. (2001), 2003du; Leonard et al. (2005), 2005hk; Chornock et al. (2006).

^d SC = Super-Chandra Candidates

^e References—(B89) Barbon et al. 1989; (B83) Branch et al. 1983; (B03) Branch et al. 2003; (E-R06) Elias-Rosa et al. 2006; (F99) Fisher et al. 1999; (F09) Foley et al. 2009; (F10a) Foley et al. 2010a; (F10b) Foley et al. 2010b; (Gara04) Garavini et al. 2004; (Gara05) Garavini et al. 2005; (Gara04) Garavini et al. 2004; (H00) Hernandez et al. 2000; (H07) Hicken et al. 2007; (H06) Howell et al. 2006; (K93) Kirshner et al. 1993; (K05) Kotak et al. 2005; (L99) Li et al. 1999; (L01) Li et al. 2001; (L03) Li et al. 2003; (M11) Marion et al. 2011; (M08) Matheson et al. 2008; (Matt05) Mattila et al. 2005; (M01) Mazzali 2001; (Mazz05) Mazzali et al. 2005; (M10) McClelland et al. 2010; (M11) Marion et al. 2011; (P07) Pastorello et al. 2007; (P96) Patat et al. 1996; (P87) Phillips et al. 1987; (P08) Pignata et al. 2008; (P10) Poznanski et al. 2010; (Q06) Quimby et al. 2006; (Q07) Quimby et al. 2007; (S08) Sahu et al. 2008; (S01) Salvo et al. 2001; (S96) Sadakane et al. 1996; (S10) Scalzo et al. 2010; (S07) Stanishev et al. 2007; (S05) Stehle et al. 2005; (T08) Taubenberger et al. 2008; (T07) Thomas et al. 2007; (T96) Turatto et al. 1996; (T98) Turatto et al. 1998; (V03) Valentini et al. 2003; (W06) Wang et al. 2006; (W09) Wang et al. 2009; (W94) Wells et al. 1994; (Y09) Yamanaka et al. 2009a; (Z10) Zhang et al. 2010.

Table 3
SYNOW Fit Parameters

Supernova Name	Epoch (days)	v_{phot} (km s ⁻¹)	C II ^a		Si II ^a	
			Velocity	τ	Velocity	τ
SN 1990N	-14	13,000	16,000	0.60	>14,000 ^b	0.50
	-8	11,000	14,000	0.25	11,000	1.40
	-2	11,000	14,000	0.15	11,000	16.0
	2	11,000	14,000	0.35	11,000	16.0
SN 1994D	-11	14,000	14,000	1.30	>14,000	14.0
	-10	13,000	14,000	0.45	>13,000	12.0
	-8	13,000	14,000	0.45	>13,000	6.00
SN 1996X	-5	12,000	14,000	0.20	>12,000	6.00
	-4	13,500	13,500	0.60	13,500	15.0
	-2	13,000	13,000	0.40	13,000	13.0
SN 1998aq	-1	12,000	13,000	0.04	13,000	8.00
	-9	12,000	15,000	0.20	13,000	2.10
	-8	12,000	14,000	0.20	13,000	2.10
SN 1999ac	0	12,000	13,500	0.60	12,000	9.00
	-15	13,000	17,000	0.40	15,000	2.00
	-9	14,000	17,500	0.30	14,000	3.00
SN 1999by	-5	12,000	14,500	0.50	12,000	12.0
	-4	12,000	14,500	0.30	12,000	13.0
	-3	12,000	14,500	0.30	12,000	14.0
SN 2001V	-7	8000	12,000	0.15	8000	1.60
	-6	8000	12,000	0.15	8000	1.60
	-4	8000	12,500	0.15	8000	1.80
SN 2003du	-13	14,000	14,000	0.60	>14,000	>4.00
	-11	12,000	14,000	0.60	>12,000	>4.50
SN 2005hk	-5	6000	7500	0.07	7000	0.30
	0	6000	7500	0.14	7000	0.70
SN 2006D	-7	11,000	14,500	0.30	13,000	0.70
	-5	11,000	14,500	0.20	13,000	0.70
SN 2006bt	-4	6500	6500	0.30	>11,000	>0.50
	-3	6500	6500	0.25	>11,000	>0.70
SN 2006gz	-14	12,000	18,500	0.50	16,500	1.10
	-12	12,000	18,500	0.40	16,500	1.50
	-10	12,000	17,500	0.30	16,000	1.60
SN 2007if	-9	8500	9500	0.25	8500	0.30
SN 2008ha ^c	-1	1000	1000	1.00	2500	10.0
SN 2009dc	-8	8000	11,000	0.50	10,000	0.80
	-7	8000	10,000	0.30	9500	0.50
	-6	8000	10,000	0.30	9500	0.50
	-5	7000	9500	0.30	9000	0.50
	-3	7000	9500	0.30	8500	0.50
	-2	6500	9000	0.30	8000	0.50
	-1	6500	9000	0.30	8000	0.50
	0	6500	8500	0.40	8500	1.10
	2	6500	8500	0.30	8000	0.60
	3	6000	7500	0.30	7500	0.70
	4	6000	7500	0.30	7500	0.70
	5	6000	7500	0.30	7500	0.70
	6	5500	7500	0.30	7000	0.70
	7	5500	7500	0.30	6500	0.70
	8	6000	7500	0.30	7000	0.70
9	5000	6000	0.20	7000	1.00	
15	5000	5000	0.20	6500	0.80	
SN 2009ig	-14	16,000	16,000	1.00	>16,000	>24
	-13	16,000	16,000	0.50	>16,000	>24
SN 2010Y	-7	12,000	15,000	0.50	14,000	6.00
	-6	12,000	15,000	0.50	14,000	5.00
	-3	12,000	14,500	0.50	13,000	10.0
	-2	11,500	14,000	0.50	12,500	18.0
	1	11,000	14,000	0.20	12,000	20.0
SN 2010ai	-10	13,500	14,000	1.00	13,500	2.00
	-8	12,500	14,000	0.50	12,500	1.50
PTF10icb	-10	11,000	14,500	0.10	>12,000	>1.10

^a Fits made with $T_{exc}=10,000$ K and $v_e=1000$ km s⁻¹.

^b Used two-components of Si II to fit broad Si II $\lambda 6355$ P-Cygni profiles.

^c See Valenti et al. (2009) for an alternate SYNOW fit where the origin of explosion is interpreted to be a core-collapse supernova.